The rates of starch depletion and hydraulic failure both play a role in drought-induced seedling mortality

Santiago Trueba, Noelia González Muñoz, Régis Burlett, Laurent J Lamarque, Yves Gibon, Teresa E Gimeno, Aurore Kaisermann, Camille Benard, Cédric Lemaire, Jose M Torres-Ruiz, et al.

Trueba *et al. Annals of Forest Science* (2024) 81:27
https://doi.org/10.1186/s13595-024-01246-7

INRAE

Annals of Forest Science

RESEARCH PAPER

Open Access

The rates of starch depletion and hydraulic failure both play a role in drought-induced seedling mortality

Santiago Trueba[1,2*†], Noelia González Muñoz[1,3†], Régis Burlett[1], Laurent J. Lamarque[1,4], Yves Gibon[5], Teresa E. Gimeno[6,7], Aurore Kaisermann[6], Camille Benard[5], Cédric Lemaire[1], Jose M. Torres-Ruiz[8], Lisa Wingate[6] and Sylvain Delzon[1]

Abstract

Key message The elapsed times to deplete starch concentrations and to reach a null hydraulic safety margin were related to tree seedling mortality under experimental drought. Starch concentration showed an accelerated decline across all species during the early stages of dehydration, while the concentrations of soluble sugars and total non-structural carbohydrates remained stable. Concomitant carbohydrate depletion and hydraulic failure drive seedling mortality under drought.

Context Current upsurges of drought events are provoking impacts on tree physiology, resulting in forest mortality. Hydraulic dysfunction and nonstructural carbohydrate (NSC) depletion have been posited as the main mechanisms leading to plant mortality under drought.

Aims This study explores the dynamics of the two mortality-inducing processes during drought stress using an experimental approach with 12 evergreen tree species.

Methods Seedlings were subjected to drought until 100% mortality was observed. Midday (Ψ_{MD}) and predawn (Ψ_{PD}) water potentials, xylem pressure leading to a 50% loss of hydraulic conductivity (Ψ_{50}), along with NSC concentrations in different organs (leaves, stems, and roots) were measured regularly during drought.

Results Total NSC concentrations and soluble sugar pools did not decline during drought. However, starch pools showed strong reductions early during drought stress as Ψ_{PD} decreased, and the time leading to starch depletion emerged as a strong mortality predictor. Ψ_{50} alone did not provide an accurate estimate of mortality, while the elapsed time to reach a null hydraulic safety margin (Ψ_{MD}—$\Psi_{50}=0$) was related to seedling mortality.

Conclusion Adopting a dynamic approach by estimating the times to consume both starch reserves and hydraulic safety margins is highly relevant to improve predictions of tree mortality under the current context of increasing global drought.

Handling editor: Maurizio Mencuccini

†Santiago Trueba and Noelia González Muñoz contributed equally to this work.

*Correspondence:
Santiago Trueba
santiago.trueba@ird.fr
Full list of author information is available at the end of the article

Keywords Embolism vulnerability, Fructose, Nonstructural carbohydrates, Hydraulic safety margin, Light environment, Sucrose

1 Introduction

Ongoing shifts in temperature and rainfall are provoking increasingly prolonged periods of drought stress and aridity-driven changes in forest structure and function (Berdugo et al. 2020). In this global change context, forest dieback and shifts in tree growth across many ecosystems are being observed as a direct consequence of the physiological stress exerted by drought intensity and frequency (Greenwood et al. 2017; Jump et al. 2017; Brodribb et al. 2020), with mortality events further exacerbated by the combination of increasing heat and drought (Hammond et al. 2022). Consequently, a large research effort is underway to elucidate the range of mechanisms that modulate drought-induced plant mortality and survival, in order to better predict mortality events and biodiversity loss (McDowell et al. 2022). For instance, it is widely accepted that plant hydraulic function is impacted by drought and can contribute significantly not only to plant survival (Choat et al. 2012; Anderegg et al. 2015a; Adams et al. 2017; Mantova et al. 2022) but also to other key ecological processes (Torres-Ruiz et al. 2024). In this context, the "hydraulic safety margin" (HSM), which is the difference between water potential minima reached during diurnal cycles and the water potential leading to hydraulic dysfunction (Ψ_{50}), is an important parameter that indicates the hydraulic operational status of a plant species in a given environment (Meinzer et al. 2009). Further, a recent study has used HSM to predict tree mortality occurrence (Sanchez-Martinez et al. 2023). Remarkably, many plants operate within narrow HSMs across a range of biomes, suggesting a widespread occurrence of hydraulically risky strategies by plants to operate close to their physiological limits and respond to rapid changes in the environment (Choat et al. 2018). Therefore, it is important to understand the pace at which plants reach a critical HSM during events of extreme drought stress and its potential implications on plant mortality (Benito Garzón et al. 2018).

Despite the current consensus on the importance of plant hydraulics on vegetation responses to drought stress, plant mortality is rather multi-factorial and hydraulic failure can be accompanied by other factors such as an increased vulnerability to biotic stressors (Logan et al. 2003; Anderegg et al. 2015b). Along with factors such as catastrophic hydraulic failure and vulnerability to pathogens, prolonged stomatal closure during drought increases the probability of mortality through the depletion of nonstructural carbohydrate (NSC) reserves used in respiration (Choat et al. 2018). The so-called "carbon-starvation" hypothesis predicts that by closing stomata, the plant reduces the risk of hydraulic failure; however, this also causes important declines in photosynthetic carbon uptake leading to "starvation" at a critical moment of increased metabolic demand for stored NSCs (McDowell et al. 2008, 2022). Experimental multifactorial studies to investigate the relative importance of hydraulic dysfunction and NSC depletion during drought stress are therefore crucial to refine our understanding of tree mortality.

Nonstructural carbohydrates (NSC) are essential sources of energy for plant growth and reproduction since they are involved in all functional processes of primary and secondary metabolism (Hartmann and Trumbore 2016). Moreover, NSCs are also important for survival acting as buffers countering environmental stress (Blumstein et al. 2022). For instance, stored NSC plays a main role in resprouting following climate stress events such as frost and drought but also following disturbances such as fire or herbivory (Bond and Midgley 2001). Given the essential role of NSC in maintaining plant function and persisting disturbance, NSC depletion might be one of the main causes of tree mortality under prolonged periods of drought. Yet, there are considerable knowledge gaps in understanding NSC storage dynamics, in particular during environmental stress (Hartmann et al. 2020). Moreover, the interaction between NSC depletion and mortality risk, and how this relationship varies among different plant taxa and drought conditions, is not clear (Sala et al. 2010), as relatively few studies have made a direct assessment of the relationship of NSC content and plant survival (Dietze et al. 2014). A previous study on tropical tree seedlings proposed that higher NSC levels, induced by experimental light manipulation, can enhance plant survival after drought (O'Brien et al. 2014). Yet, another study applying a long-term experimental drought on a neotropical set of species found that NSC levels remained stable during stress, proposing hydraulic failure as the main prevalent driver of tree mortality (Rowland et al. 2015). Further, a study on the conifer tree species *Pinus edulis* showed a positive impact of NSC content on respiration rates and turgor maintenance (Sevanto et al. 2014). Similarly, a relationship between NSC content and osmotic potential was found in Douglas-fir (Sala et al. 2012). More recently, a study on *Pinus ponderosa* seedlings showed an impact of ectomycorrhizal

networks on NSC levels, suggesting an influence of NSC on water relations independent of water status (Sapes et al. 2021). Despite this previous evidence on the interaction of NSC and hydro-physiological features, the influence of plant water status on the dynamics of different NSC pools, and their allocation to different plant organs during drought stress, need to be explored on a larger set of species representing a wide phylogenetic diversity.

In this study, we aimed at investigating plant hydraulic functioning and NSC concentration dynamics, and their interaction with plant water status during dehydration, in order to identify the main ecophysiological causal factors of drought-induced mortality in 12 forest species. We conducted a factorial experiment on seedlings of these tree species aiming to manipulate NSC concentration by exposing seedlings to different light environments, expecting shaded individuals to have lower carbohydrate concentrations. Further, water stress was applied across treatments. Specifically, we assessed whether (i) light manipulation has an effect on NSC concentrations, expecting individuals from different light treatments to show divergent mortality rates under drought; (ii) NSC concentrations, distinguishing soluble sugars and starch, delayed plant mortality during drought within species and how NSC concentrations are affected by drought; we hypothesized that plants with non-depleted NSC pools would survive longer and that a progressive decline in total NSC concentration during drought will be observed, lending support for the carbon starvation hypothesis; and (iii) plants maintain relatively stable NSC concentrations while they consistently cross their HSM (i.e., showed a null or negative hydraulic safety margin) during drought, lending support for the hydraulic failure hypothesis. We assessed these aims and hypotheses in an experiment under controlled conditions performed on seedlings of eight conifer and four angiosperm tree species, spanning a gradient of drought-tolerances. Our results can help elucidate the contributing roles of hydraulic conductivity and carbon starvation as distinct or concomitant drivers of plant mortality. These observations can provide new insights into the mortality mechanisms of the studied species, shedding new light on vegetation dynamics under current environmental drought stress.

2 Materials and methods

2.1 Plant material and species selection

We selected 12 tree species, eight gymnosperms and four evergreen angiosperms (Appendix Fig. 10) with differing hydraulic sensitivities, based on species assessments of embolism resistance (Table 1). The xylem pressure at which 50% loss of xylem conductivity occurs, Ψ_{50}, is a common index to measure vulnerability to cavitation and embolism, which is obtained by measuring the loss of hydraulic conductivity as a function of the tension in xylem sap (vulnerability curve). The vulnerability curves were measured at the Phenobois platform (INRAE, University of Bordeaux; Pessac, France) using the Cavitron technique (Cochard 2002; Burlett et al. 2022) on branches from individuals not included in the drought experiment.

Table 1 List of studied species including mortality, hydraulic vulnerability, and starch depletion thresholds. Hydraulic safety, starch concentration, and mortality time thresholds after shade- and light-exposed treatments in the light manipulation phase are included. Additional information is available in Appendix Tables 5, 6, and 7. Phylogenetic relationships across species are shown in Appendix Fig. 10. Ψ_{50}, the water potential inducing 50% of loss in hydraulic conductivity; $time_{mortality50\%}$, time leading to 50% of plant mortality; $time_{HSM0}$, the time to reach a null safety margin (Ψ_{MD}—Ψ_{50}); $time_{starch50\%}$, time leading to 50% of starch depletion

Species	Family	Clade	Ψ_{50} (MPa)	$Time_{mortality50\%}$ (days)		$Time_{HSM0}$ (days)		$Time_{starch50\%}$ (days)	
				Shade	Light	Shade	Light	Shade	Light
Abies nordmanniana Steven (Spach)	Pinaceae	conifer	−3.65	41.37	36.75	59.01	49.84	37.23	37.74
Arbutus unedo L	Ericaceae	angiosperm	−8.23	46.9	20.44	77.49	65.59	39.21	29.55
Buxus sempervirens L	Buxaceae	angiosperm	−8.00	66.43	57.26	99.12	84.28	42.15	40.04
Cedrus atlantica (Endl.) Manetti ex. Carrière	Pinaceae	conifer	−5.14	60.97	43.47	112.28	77.63	48.75	57.26
Cupressus macrocarpa (Hartw.) Bartel	Cupressaceae	conifer	−6.73	68.46	43.75	117.18	77.84	50.62	55.68
Ilex aquifolium L	Aquifoliaceae	angiosperm	−6.60	62.72	56.63	115.64	123.9	52.62	50.83
Juniperus thurifera L	Cupressaceae	conifer	−9.29	89.25	85.75	122.15	140.49	55.78	55.61
Pinus halepensis Mill	Pinaceae	conifer	−5.03	65.52	62.51	116.41	100.45	69.13	50.58
Pinus pinaster Aiton	Pinaceae	conifer	−3.70	85.12	79.1	156.03	116.55	69.19	67.35
Pinus sylvestris L	Pinaceae	conifer	−3.19	83.02	70.14	111.51	82.74	56.62	57.30
Quercus ilex L	Fagaceae	angiosperm	−7.13	49.35	55.93	72.66	71.82	42.61	44.38
Tetraclinis articulata (Vahl) Mast	Cupressaceae	conifer	−13.13	68.74	56.35	112.07	114.8	62.83	59.88

Data describing the vulnerability of xylem embolism for the angiosperm species *Buxus sempervirens* L. and *Ilex aquifolium* L. were obtained from the metadata of Choat et al. (2012). In our experiment, angiosperms Ψ_{50} ranged from − 6.60 MPa in *Ilex aquifolium* to − 8.23 MPa in *Arbutus unedo* L. For the selected gymnosperms, Ψ_{50} values ranged from − 3.19 MPa in *Pinus sylvestris* L. to − 13 MPa in *Tetraclinis articulata* (Vahl) Mast.

2.2 Experimental design and procedures

From February to November 2016, we conducted a factorial design experiment with two independent factors: NSC concentration and water stress. The experiment was carried out in a greenhouse at the INRAE Forest Research Station (0° 45′ 58.60W, 44° 44′ 18.6N, Cestas, France). Environmental conditions inside the greenhouse were monitored by a temperature and air relative humidity sensor (CS215, Campbell Scientific, Logan, USA) and quantum sensors (SP110, Apogee Instrument, Logan, USA). Data were logged hourly on a datalogger (CR1000, Campbell scientific, Logan, USA). In February 2016, 156 one-year-old plants per species, grown under optimal watering conditions, were acquired from different nurseries in Spain (*Juniperus thurifera* L. and *Tetraclinis articulata*) and France (remaining species; PlanFor nursery, Uchacq-et-Parentis). Plants were transplanted to 14 × 14 cm, 3 l pots filled with commercial substrate consisting of a volumetric mix of 3:2:2:1 quantities of bark, peat, soil, and fertilizer (15% N, 8% phosphoric anhydride, 11% potassium oxide and oligo elements), respectively. Pots were randomly distributed and left to acclimate in the greenhouse under well-watered conditions until early March 2016. During the acclimation period, all plants were kept watered to field capacity. Pesticides were applied during the total experimental period to prevent fungal or insect infections. The experiment had two phases: a first light manipulation phase and a subsequent drought experiment (Fig. 1).

2.2.1 Phase 1: Light manipulation

After an initial period of 36 days of acclimation to greenhouse conditions (Fig. 1), we started applying two different light treatments to induce a shift in total NSC concentration between experimental treatments within plants of the same species, following previously published procedures (O'Brien et al. 2014). Inside the greenhouse, half of the plants of each species were randomly placed under high-light conditions (full-sun irradiance, sometimes supplemented with artificial light to aim for 12 h of light). The other half of the plants of each species were placed under a shade net reducing incident sun-light by 50%, and with no supplement of artificial

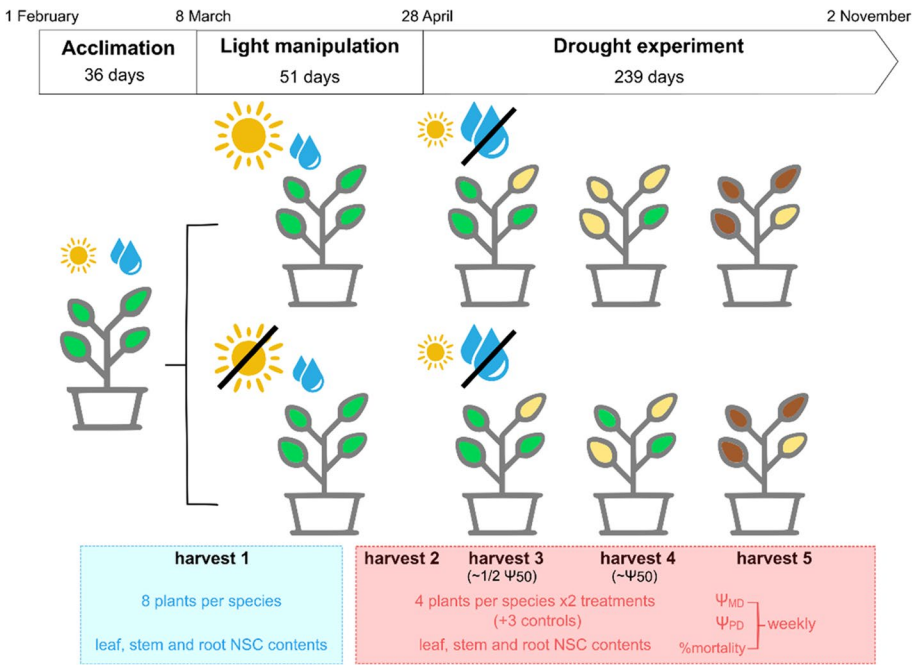

Fig. 1 Experimental design applied on 12 angiosperm and conifer species. The first acclimation period was followed by a light manipulation phase, and a drought experiment until full mortality was observed. Five harvests were carried out to gather NSC data from three different organs. The number of harvested plants per species and per treatment are indicated inside the lower boxes. Additional measurements of predawn (Ψ_{PD}) and midday (Ψ_{MD}) water potentials along with visual assessments of mortality percentages based on leaf coloration were carried out weekly during the drought experiment

light, in an attempt to enrich and deplete NSC concentrations in the potted seedlings, respectively (Fig. 1). Incident light intensity was calibrated under both light treatments before the beginning of the experiment with a portable light meter (LI-250A, Licor, Lincoln, NE, USA). After 1 month, we initially tested the NSC concentration of the plants to assess whether the different light treatments were having an impact on NSC concentrations. This consisted of collecting 2–3 leaves in the morning before 06:00, from 10 randomly selected plants per species. The leaves were then pooled together and analyzed for their soluble sugar and starch concentrations (see below for the NSC analysis procedures). Based on the results obtained, we increased the shade conditions (up to 80% of shade) for a total of 51 days of light manipulation treatment. Furthermore, to avoid significant biomass and transpirative surface differences across the light treatments, we trimmed individuals to maintain equivalent leaf surface areas between treatments. Watering to field capacity two times per week was applied during the light manipulation phase.

2.2.2 Phase 2: Drought treatment

On April 28, 2016, we removed the shade net, stopped the artificial light, and started the drought treatments (Fig. 1). On day 1 of phase 2, all pots were submerged in water, to start the treatments under equally water-saturated soil conditions. Plants of each species within each light treatment were randomly allocated into a watering treatment, resulting in four experimental treatments: control-light (regular watering and high light), control-shade (regular watering and shade), drought-light (withheld watering and high light), and drought-shade (withheld watering and shade). Control pots were maintained at field capacity, whereas water was withheld from the drought pots until the end of the experimental period when 100% of plant mortality was observed (see below).

2.3 Harvests, data collection and mortality estimations

Predawn (Ψ_{PD}) and midday (Ψ_{MD}) water potentials were measured weekly with a Scholander pressure chamber (Precis 2000, Gradignan, France) from the beginning of the drought treatment and until the water potential of each plant species fell below the limit of the pressure chamber at − 10 MPa. Hydraulic safety margins (HSM) were continuously estimated as the difference between Ψ_{MD} and Ψ_{50}. In every water potential measurement campaign, we measured up to eight plants per species, including one control plant and at least three per drought-light treatment. We performed five harvests of whole plants during the experimental period (Fig. 1). Plant mortality was assessed weekly from June 15 until November 2, 2016, by which point all plants in the drought treatment were considered dead. Mortality was visually estimated from the percentage of dead leaves per plant assessed by observing changes in leaf coloration. The first and second harvests were performed before and right after the light manipulation treatment, respectively. Two further harvests (harvests 3 and 4) were performed when the leaf water potentials reached nearly half of the Ψ_{50} and at the Ψ_{50} of the species, respectively. Finally, a last harvest was completed (harvest 5) when at least 25% of the individuals of a species were considered dead (i.e., having 100% of dead leaves). In harvest 1, we harvested eight plants per species. In harvest 2, we collected four plants per species and light treatment. From harvests 3 to 5, we collected three plants per control-treatment and four plants per drought-light treatment. From every harvested plant, we took a 3 g subsample of leaves, stem, and roots for NSC concentration analysis; we also determined the total dry mass of leaves, stem, and roots. Dry masses were used to estimate above-ground and below-ground biomasses, along with root-to-shoot ratios, to control for potential changes in biomass allocation across treatments under severe drought (Trueba 2024).

2.4 Non-structural carbohydrate (NSC) analyses

Each subsample of 3 g taken from stems, leaves, and roots per harvested plant was immediately immersed in liquid N after collection and then stored at − 80 °C. Samples were ground to homogeneity in cryogenic conditions and 20 mg aliquots were weighted. NSC concentration was determined at the *Bordeaux Metabolome* HiT-ME platform at INRAE-Bordeaux (Villenave d'Ornon, France). Extraction was performed via ethanolic fractionation, in which the material was extracted at 80 °C for 20 min using 80% ethanol twice then 50% ethanol once (volumes were 250, 150, and 250 µl, respectively). Fructose, glucose, sucrose, and starch amounts were determined enzymatically in ethanolic extracts following the procedure described in Stitt et al. (1989) and in Hendriks et al. (2003). For both soluble carbohydrates and starch, a final concentration of 1% polyvinylpyrrolidone (w:v) was added to the assay mix to prevent inhibition of the enzymes used for the determination. Extractions and assays were performed in 96 well microplates using a Star pipetting robot (Hamilton, Villebon-sur-Yvette, France), and the absorbances were read at 340 nm in MP96 readers (SAFAS, Monaco). The sum of fructose, glucose, and sucrose concentrations was employed to estimate soluble sugar concentrations.

2.5 Statistical analyses

Comparisons of total NSC (soluble sugars + starch) concentrations across light treatments prior to the drought phase and comparisons of NSC concentrations across

plant organs during the drought phase were carried out for each species with unpaired two-sample *t* tests and one-way ANOVA with post hoc Tukey's honest significant differences using 95% confidence intervals. Assumptions of residual homogeneity and normality were tested prior to analyses. Similar methods were used to assess differences in biomass allocation under severe drought (harvest 5) across treatments. A model explaining total NSC variance including the interaction light treatment × species was also performed to assess if light manipulation treatments had an effect on total NSC concentrations across all species. Differences in survival probabilities after drought between light treatments were analyzed using the Kaplan–Meier method, which is a non-parametric approach resulting in a step function, where there is a step down each time a mortality event occurs. A log-rank test was used to compare survival times between treatments. Furthermore, we employed a Cox regression model, a semi-parametric model used to fit regression models that have survival outcomes, to account for the effect of light treatments on individual survival. Kaplan–Meier curves and Cox regression models were implemented with the "survival" and "survminer" packages (Fox 2002; Kassambara et al. 2017). We constructed curves for the temporal dynamics of mortality probability, hydraulic safety margins (HSM), and starch depletion using the maximum likelihood selection of model parameters with the "likelihood" package. We assessed the performance of different functions based on their higher coefficients of determination and lower Akaike information criterion corrected for small *n* (AICc) (Burnham and Anderson 2003). Logistic functions on the relationship of mortality percentage over time, and linear functions on the relationship of HSM and starch depletion over time provided the best fits. The logistic and linear fits were then used to estimate the time leading to 10%, 50%, and 80% of plant mortality ($time_{mortality10}$, $time_{mortality50}$, $time_{mortality80}$), the time leading to a null HSM ($time_{HSM0}$) and to 50% starch depletion ($time_{starch50}$). We estimated stomatal behaviors by assessing the parameters of the linear relationships between midday (Ψ_{MD}) and predawn (Ψ_{PD}) water potentials (Martínez-Vilalta et al. 2014), measured along the drought experiment. Linear and nonlinear regressions, along with Pearson's correlations, were employed to estimate the strength of bi-variate relationships. Additionally, to predict plant mortality based on starch depletion and HSM variables across species, we used phylogenetic generalized least-squares analyses (PGLS) with a lambda (λ) maximum likelihood optimization to control for phylogenetic non-independence between related species (Felsenstein 1985; Freckleton et al. 2002). Data of different light treatments was species-averaged prior to PGLS analyses. Phylogenetic relationships, including branch length calibrations and divergence times, were obtained from published data (Magallón et al. 2015; Smith and Brown 2018). The assemblage of the tree with the phylogenetic relationships of the 12 studied species (Appendix Fig. 10) was carried out using the package "ape" (Paradis and Schliep 2018) and PGLS models were fit using the package "caper" (Orme et al. 2018). All analyses were considered significant at $\alpha = 0.05$. All statistical analyses and data treatment were performed using R v.3.6.3 (R Core Team 2020).

3 Results

3.1 Variability of NSC concentrations under different light treatments across species and organs

In response to the light treatments only four species showed significant differences between total NSC concentration at harvest 2 (Fig. 1). One angiosperm, *Ilex aquifolium*, and two conifers, *Abies nordmanniana* Steven (Spach) and *Pinus halepensis* Mill., showed decreases in total NSC in shaded individuals (Fig. 2; Appendix Table 2), while *Cupressus macrocarpa* (Hartw.) Bartel individuals growing under the shaded treatment showed higher amounts of total NSC (Fig. 2; Appendix Table 2). The remaining species showed only slightly higher NSC levels following the light treatment (Fig. 2; Appendix Table 2). A linear model explaining total NSC variance including the light treatment × species interaction showed that the species effect better explained total NSC variations rather than the light treatments (Appendix Table 3). Similarly, pre-drought NSC concentration barely differed between light treatments when analyses were conducted within each organ (Appendix Fig. 11). Stem NSC was more variable with four species differing significantly between light treatments, while only a single species showed differences in total NSC in leaves and roots between light treatments (Appendix Fig. 11; Appendix Table 4). Shifts in total NSC at the organ level following the light manipulation phase differed and never co-occurred in more than one organ for the same species (Appendix Fig. 11; Appendix Table 4).

3.2 Starch depletion and lack of total NSC and soluble sugar consumption

Water status influenced starch dynamics in all species, such as indicated by the relationship of starch concentration with Ψ_{PD}, showing a strong exponential decline of leaf starch concentration with decreasing Ψ_{PD} (Fig. 3). Starch concentration was linked to Ψ_{PD}, while leaf soluble sugars concentration was unaffected by Ψ_{PD} variation (Fig. 3). Indeed, soluble sugars remained equal, eventually showing slight declines or increases as Ψ_{PD} declined, but these relationships were non-significant

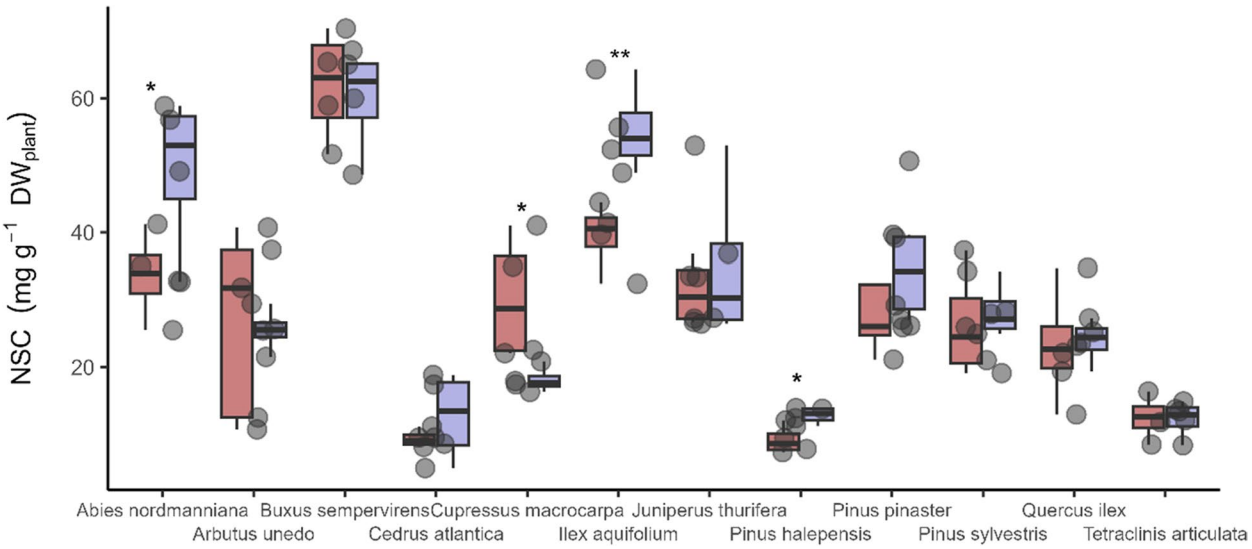

Fig. 2 Comparisons of total non-structural carbohydrate (NSC) concentrations in 12 studied angiosperm and conifer species after the light manipulation phase. NSC values for light-exposed (blue) and shaded (red) individuals of each species are shown. Boxes and bars show the median, quartiles, and extreme values. Dots are individual data points. Significant differences between light treatments are indicated: *$p \leq 0.05$; **$p \leq 0.01$. See Appendix Table 2 for additional statistics from the comparison of NSC levels of different light treatments

overall (Fig. 3). Such interactions of water potential with starch and soluble sugar concentrations were rather similar regardless of the light treatment applied prior to the drought experiment (Appendix Figs. 12, 13). A weak effect of water status on plant total NSC concentrations was also observed with no overall relationships found with Ψ_{PD} (Fig. 4). Only *Abies nordmanniana* and *Buxus sempervirens* displayed significant declines in total NSC with decreasing water potentials, regardless of the pre-drought light treatment considered (Fig. 4). Pre-drought light manipulations did not seem to have any important effect on NSC dynamics during dehydration as indicated by the strong overlap in individuals from both treatments during dehydration (Fig. 4).

3.3 NSC concentrations at different organ levels, hydraulic strategies and shifts of biomass allocation under drought

Poor and inconsistent relationships between total NSC concentration and water potential were also observed when considering NSC concentrations in different organs (Appendix Figs. 14-16). Further comparisons of NSC concentrations across organs showed that leaves had higher total NSC concentrations than stems and roots before the onset of the drought stress (Fig. 5a–c). This was principally driven by the higher concentration of soluble sugars in leaves (Fig. 5c), while starch concentrations were equal among the three organs (Fig. 5b). During severe drought stress, 110 days after the onset of the drought treatment (harvest 5), ranks of NSC concentration remained relatively similar when considering total NSC, and soluble sugar concentrations (Fig. 5d, f). Starch concentrations showed strong declines and roots retained more starch than leaves and stems after severe stress (Fig. 5e).

Regarding the hydraulic drought response strategies of species, most of the variability in Ψ_{MD} was explained by Ψ_{PD}, with both variables showing very tight relationships. Slopes of the $\Psi_{MD} \sim \Psi_{PD}$ were ≤ 1 in most species, suggesting partial stomatal control to water loss with strong coordination between the gas and liquid phases of water transport (Appendix Fig. 17). The conifers *Juniperus thurifera* and *Pinus sylvestris* appeared to have a less strict stomatal control (Appendix Fig. 17). Plants under both treatments showed slight losses of above-ground biomass under severe drought stress as compared to control individuals (Appendix Fig. 18a). Below-ground biomass and root to shoot ratios remained equivalent across droughted light treatments and control plants (Appendix Fig. 18b,c). At the onset of drought, all species showed higher above-ground biomasses in individuals under the light treatment, with the exceptions of *A. nordmanniana* and *Q. ilex* (Appendix Fig. 19), which had higher above-ground biomasses in individuals from the shade treatment.

3.4 Tree seedling mortality rates under drought across light treatments

Light-exposed individuals showed earlier mortality than those from the shaded treatment overall (Table 1;

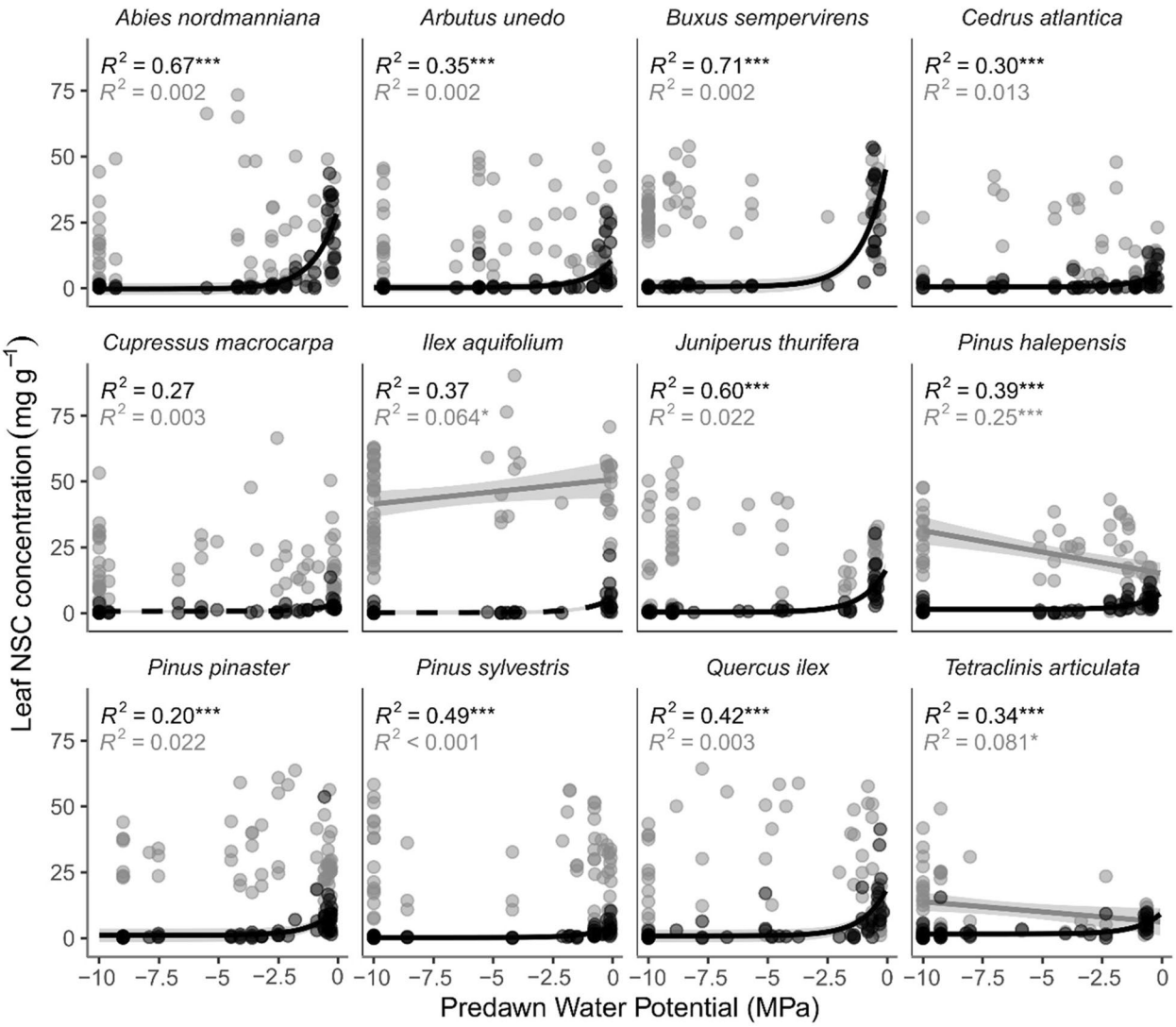

Fig. 3 Leaf soluble sugars and starch dynamics as a function of predawn water potential. Dots represent soluble sugars (gray) and starch (black) concentrations for individual leaf measurements along the dehydration experiment. Solid regression lines and 95% confidence intervals (gray-shaded areas) are included in significant relations. Coefficients of determination for each NSC type are included following the same color code. Soluble sugar concentration results from the sum of fructose, glucose, and sucrose concentrations. *0.01 < P < 0.05; ***P < 0.001. Additional figures depicting starch and soluble sugar concentration dynamics and distinguishing different light treatments are available in Appendix Figs. 12 and 13

Fig. 6; Appendix Fig. 20). The only species that showed a different behavior was *Quercus ilex* L., where shaded individuals showed earlier mortality (Table 1; Appendix Fig. 20). Interestingly, the trend of earlier mortality in light-exposed individuals was also observed in *A. nordmanniana*, *I. aquifolium*, and *P. halepensis*, species that exhibited effective NSC enrichments after the light manipulation phase. On average, light-exposed individuals reached mortality thresholds 10.5 days sooner. Across species, the average times to reach 10%, 50%, and 80% mortality in individuals from the pre-shaded treatment were 48.3, 65.6, and 76.3 days, respectively. For the individuals under the full light pre-treatment, average times to reach 10%, 50%, and 80% mortality were lower, with estimations of 39.9, 55.7, and 65.8 days, respectively. Mortality curves for each species, depicting percentage mortality over time, are available in Appendix Fig. 20. Time thresholds at different mortality levels for all species and treatments, along with model parameters are included in Appendix Table 5.

Individuals of all species reached 100% mortality, as indicated by the employed proxy of full foliage mortality,

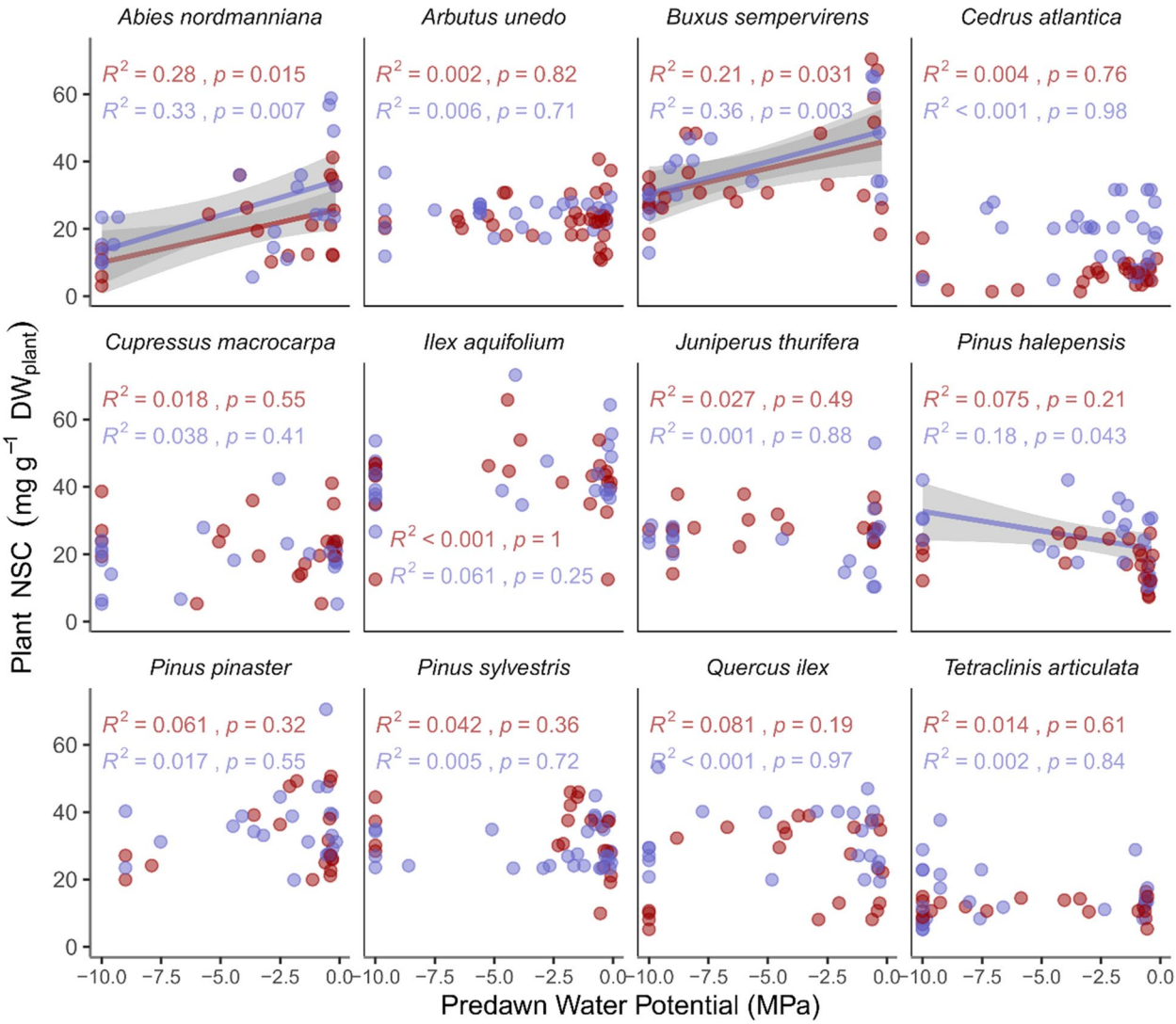

Fig. 4 Total nonstructural carbohydrate concentrations as a function of predawn water potential. Different colors in dots and lines correspond to light-exposed (blue) and shaded (red) individuals before the drought experiment. Solid regression lines and 95% confidence intervals (gray-shaded areas) depict significant relationships. Coefficients of determination and *p* values are included for each light treatment. Similar figures of total NSC concentration dynamics as a function of predawn water potential for three different organs are provided in Appendix Figs. 14–16

at the end of the drought experiment (Fig. 6; Appendix Fig. 20). *Arbutus unedo* was the species that reached mortality earliest (Table 1), with four individuals in the light pre-treatment reaching full mortality after only 48 days elapsing between the start of the drought experiment and the mortality event. *Juniperus thurifera* was the species that reached full mortality at the latest (Table 1), with three individuals reaching full mortality 188 days after the onset of the experiment. According to a log-rank test to compare survival times between treatments, we observed a significant difference (X^2 (1 df) = 31.9, $p \leq 0.001$), showing lower survival rates for individuals from the light pre-treatment for an equal amount of elapsed time relative to individuals grown under shade (Fig. 6). Additionally, a Cox regression also showed significant differences in the hazard ratio (HR) between the light treatments, indicating that around 1.48 times more light-exposed individuals die than individuals grown in shade before drought, along any given time during the drought experiment (HR = 1.48; 95% CI = 1.28,1.70; $p \leq 0.001$).

3.5 Hydraulic safety margins and starch depletion as predictors of mortality rates

Hydraulic safety margins ($HSM = \Psi_{MD} - \Psi_{50}$) declined significantly over time during the dehydration

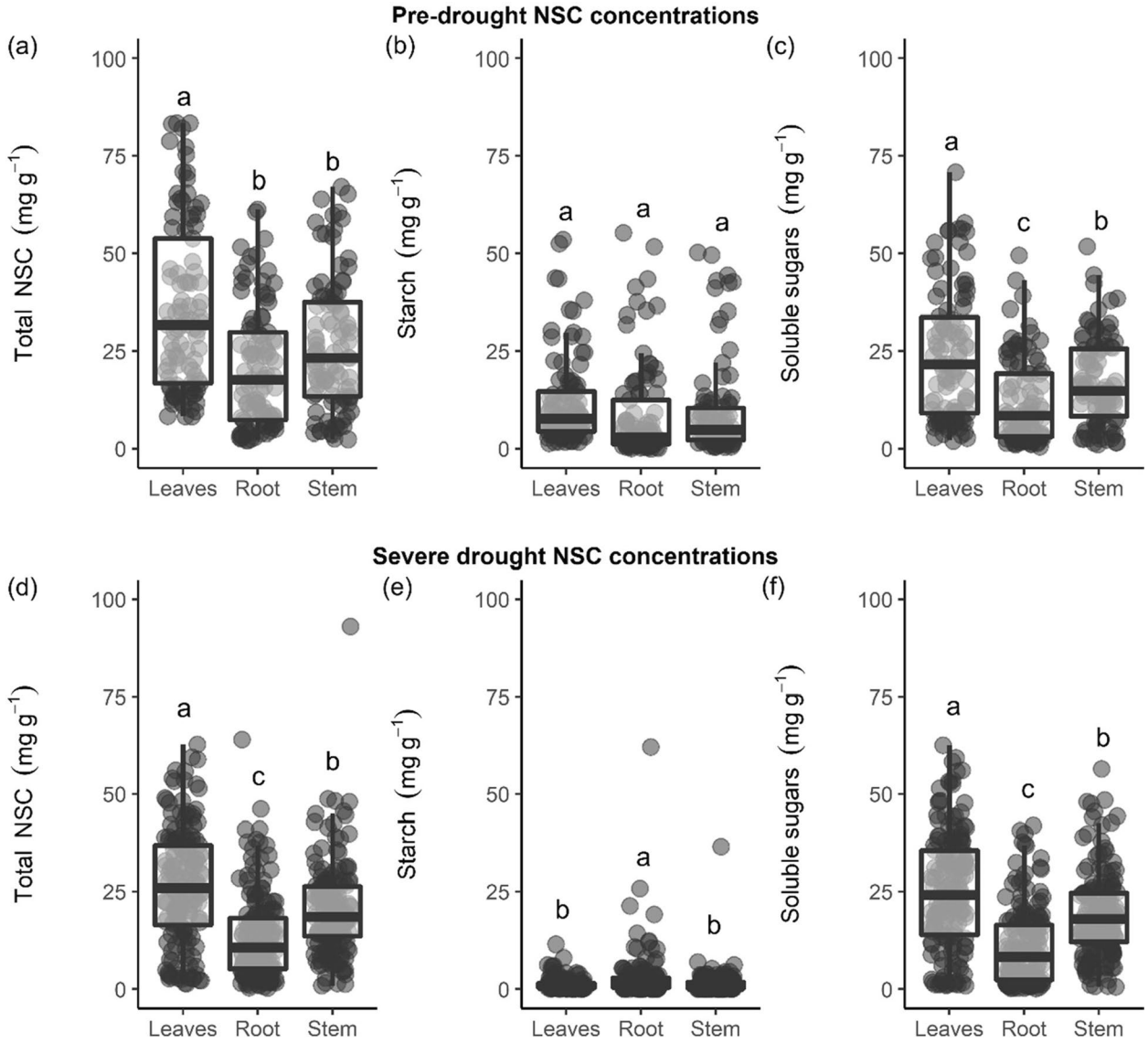

Fig. 5 Comparisons of non-structural carbohydrates (NSC) concentrations across plant organs. NSC concentrations in 12 species before drought stress (**a**–**c**) and after severe drought stress (**d**–**f**). Soluble sugars include fructose, glucose, and sucrose. Measurements correspond to harvest 2 (**a**–**c**) and harvest 5 (**d**–**f**), see "Materials and Methods" section for details on the experimental design. Boxes and bars show the median, quartiles, and extreme values. Data points are individual measurements. Letters indicate significant differences in NSC concentrations between organs

experiment (Fig. 7). Individuals that were light-exposed prior to the drought phase crossed the boundary to a negative HSM before shaded individuals for all species, with the exception of *Ilex aquifolium*, *Juniperus thurifera*, and *Tetraclinis articulata* (Fig. 7). The average elapsed time to reach a null HSM ($time_{HSM0}$) across species and light treatments was 99.1 days, with a minimum of 49.8 days in light exposed individuals of *Abies nordmanniana* and a maximum of 156 days in shaded individuals of *Pinus pinaster* Aiton (Table 1). A full report of model parameters and estimated $time_{HSM0}$ across species and treatments is available in Appendix Table 6. Given the strong declines observed in starch concentrations during drought, we further analyzed the dynamics of starch depletion over time. Total starch concentration, integrating all analyzed organs, was significantly and negatively related to elapsed time (Fig. 8). A full report of model parameters and estimated times to deplete 50% of starch concentrations ($time_{starch50}$) across species and treatments

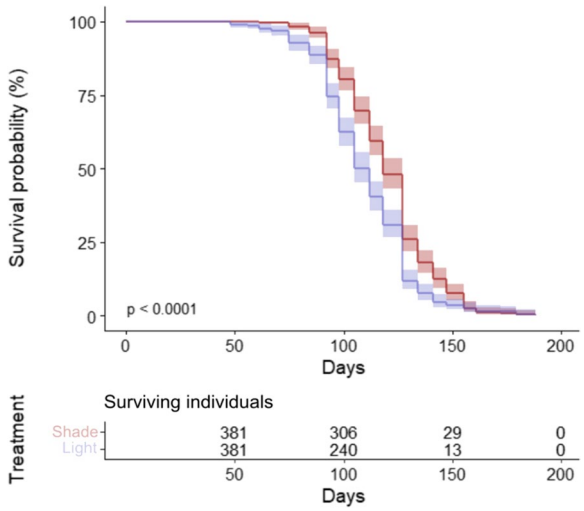

Fig. 6 Drought survival curves based on the Kaplan–Meier method comparing two different light treatments for the 12 species pooled together. Light-exposed (blue) and shaded (red) individuals are distinguished. Decreases in the number of individuals at risk for both treatments are also included. Additional curves of drought-induced mortality percentage over time are available in Appendix Fig. 20

is available in Appendix Table 7. On average, 50% of starch concentration was depleted across species and light treatments in 51.4 days, with a minimum of 29.5 days in light-exposed individuals of *Arbutus unedo* and a maximum of 69.2 days in shaded individuals of *Pinus pinaster* (Table 1).

No correlations were observed when comparing Ψ_{50} with percent mortality thresholds (Appendix Fig. 21). On the other hand, $time_{HSM0}$ was a strong predictor of estimated mortality thresholds in all species, regardless of the light conditions considered (Fig. 9a,b; Appendix Table 8). The slope of HSM over time ($slope_{HSM\sim time}$), which depicts the pace at which HSM declines over time, was also a good predictor of mortality thresholds (Appendix Table 8). $Time_{starch50}$ was also a good predictor of seedling mortality (Fig. 9c,d; Appendix Table 8), with species showing a more accelerated starch consumption reaching mortality earlier than those that were able to keep starch reserves for longer dehydration periods. Positive significant relationships between plant mortality thresholds and $time_{starch50}$ along with $time_{HSM0}$ were also supported by phylogenetic generalized least-square (PGLS) regressions (Appendix Table 9). However, $slope_{HSM\sim time}$ was less accurate in predicting mortality using PGLS (Appendix Table 9). All the performed PGLS regressions had optimized values of Pagel's lambda of $\lambda = 0$, denoting a lack of phylogenetic signal (Appendix Table 9).

4 Discussion

Under the current context of increasing drought stress and tree mortality, the mechanisms driving plant mortality need to be further elucidated. Our study shows that total NSC concentrations remained stable as drought increased and plant water potential declined, and this was mainly influenced by high and stable contents of soluble sugars during drought. However, non-soluble starch concentrations showed a strong decline, and the elapsed time to consume half of the starch reserves ($time_{starch50}$) was a good predictor of seedling mortality, highlighting the importance of this carbohydrate on plant survival. Additionally, we found that the time taken for plants to cross the hydraulic safety margin ($time_{HSM0}$) was also an explanatory trait to predict plant mortality. Our results stress the importance of starch depletion and plant hydraulic dysfunction as joint drivers of plant mortality under drought. Adopting a dynamic approach by estimating both the rates of starch consumption and the time to reach HSM are promising avenues to predict the fate of vegetation in the current context of increasing drought events.

4.1 Light manipulation effects on nonstructural carbohydrate (NSC) reserves and different NSC pools

A small amount of the acquired carbon via plant photosynthesis is retained in the form of nonstructural carbohydrates (NSC). NSC pools support metabolism during stress events when carbon acquisition is compromised but also during the night when light is not available (Dietze et al. 2014). Light deprivation was therefore expected to induce NSC depletion via reduced photosynthetic carbon resourcing. However, in our experiment, light manipulation did not result in a systematic depletion of NSC concentrations in our tree seedlings. Indeed, we observed either variable or inconsistent differences in total NSC concentrations after the light manipulation phase with only three species; *Abies nordmanniana*, *Ilex aquifolium*, and *Pinus halepensis*; showing significant decreases in total NSC after a 49-day period of light reduction. Our results contrast with those from a previous study where shading induced NSC depletion (O'Brien et al. 2014). In that experiment, O'Brien et al. (2014) applied longer shade-exposure times (198-day period of light-shade alternate light environment), on shade-tolerant tree seedlings typical of the tropical understory. Therefore, we cannot discard that the lack of NSC concentration manipulation in our study might arise from a shorter shading period or from the different shade tolerances of our species. In this context, it has been shown that only severe and prolonged shading can lead to effective NSC reduction, with shaded plants

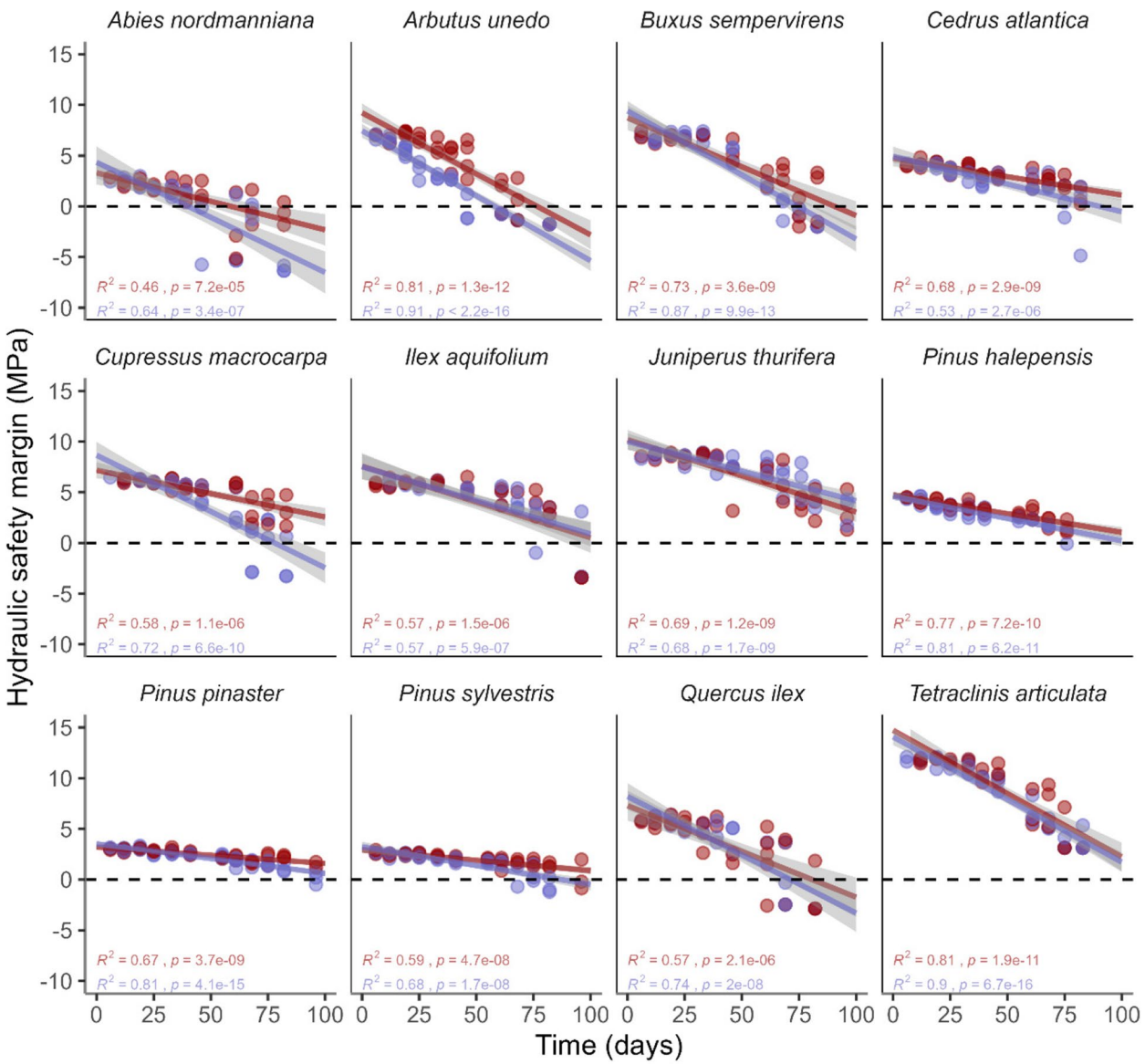

Fig. 7 Changes in hydraulic safety margin during the time along the drought experiment. Hydraulic safety margins were estimated as Ψ_{MD}—Ψ_{50}. Different colors in dots and lines correspond to light-exposed (blue) and shaded (red) individuals during the light manipulation phase before the drought experiment. Solid regression lines and 95% confidence intervals (gray-shaded areas) depict significant relationships. The horizontal dashed line corresponds to the shift between positive and negative safety margins. Coefficients of determination and *p* values are included for each light treatment. Model parameters and estimates of time at HSM = 0 are available in Appendix Table 6

keeping functional carbon storage while reducing growth (Myers and Kitajima 2007; Weber et al. 2019). Another recent study using a similar protocol of light manipulation to induce NSC depletion in *Populus nigra* saplings found that shade exposure induced NSC depletion (Tomasella et al. 2021). Yet, in Tomasella et al. (2021), this reduction was evident only for starch reserves, which were also shown to be more labile in our study, while soluble sugars also showed no differences between light treatments, consistent again with our study. Another similar study manipulating light and water availability in Douglas fir saplings (*Pseudotsuga menziesii*), also suggested that both factors led to exhaustion of carbohydrate reserves (Marshall 1986). However, that study showed rather stable sugar concentrations after dehydration in both shaded and unshaded plants, while starch concentrations were completely depleted following dehydration and regardless of the light treatment (Marshall 1986). This is in line with another study reporting that drought effects on *Pinus ponderosa* NSC concentrations respond mainly to changes in starch rather than in soluble sugar concentrations (Sapes et al. 2019). Our results therefore

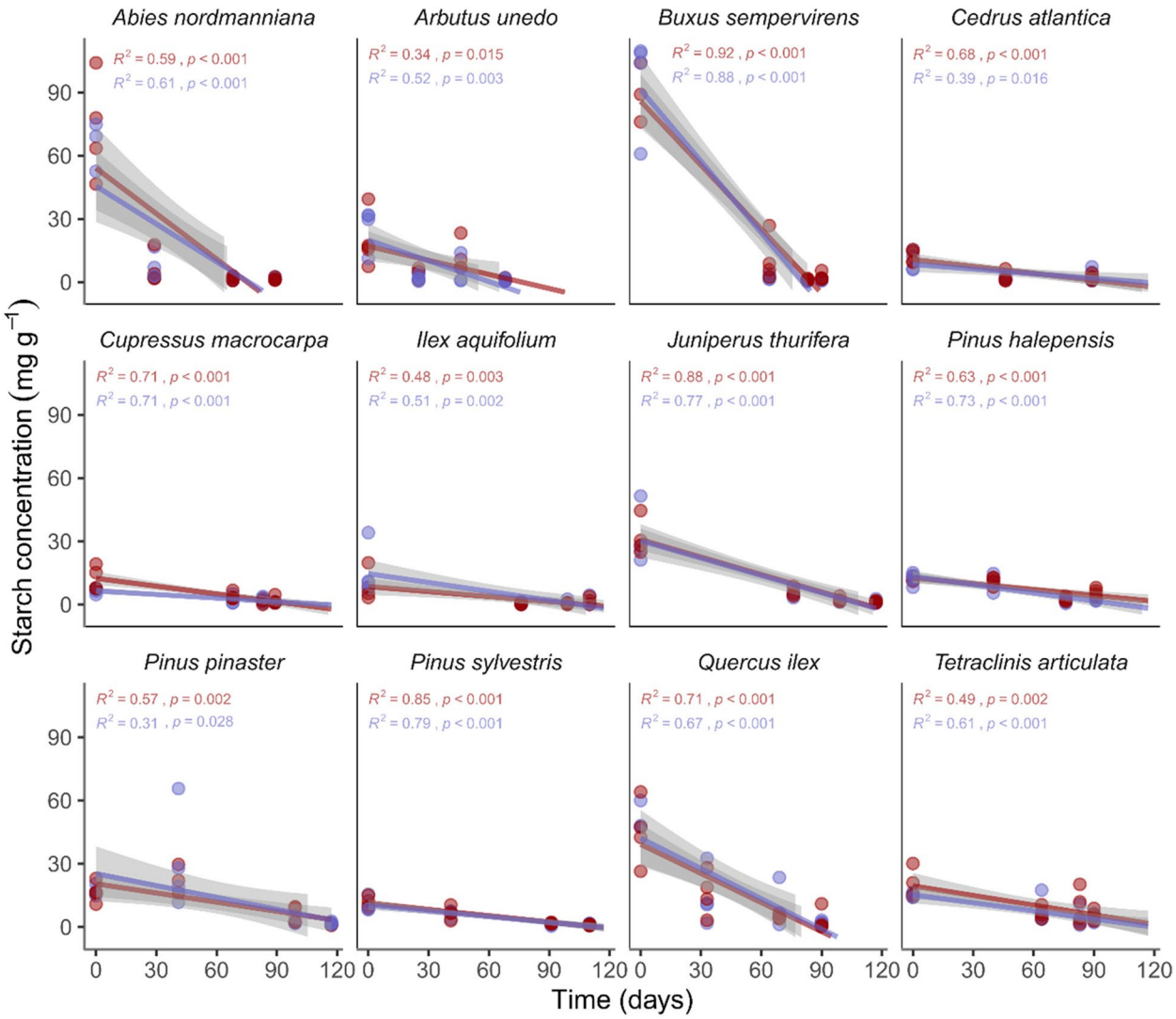

Fig. 8 Total starch concentration as a function of elapsed time. Different colors in dots and lines correspond to light-exposed (blue) and shaded (red) individuals before the drought experiment. Regression lines and 95% confidence intervals (gray-shaded areas) are included. Coefficients of determination and *p* values are included for each light treatment. Model parameters and estimations of $time_{starch50}$, the elapsed time to reach 50% of starch depletion are included in Appendix Table 7

highlight that potential differences in NSC following light deprivation and/or drought stress might stem from shifts in starch reserves with different responses of other NSC, which contribute collectively to the stabilization of NSC concentrations during light exposure and plant stress.

4.2 NSC dynamics during drought, organ allocation and the relevance of starch reserves on survival

During the drought phase of our experiment, total soluble sugar concentrations (glucose, fructose and sucrose) did not consistently decline with decreasing water potentials. Indeed, soluble sugars remained relatively stable as predawn water potentials (Ψ_{PD}) declined, showing no clear trends across species and indicating homeostatic regulation of labile sugar pools matched to energy requirements. Therefore, the weak influence of plant water status on soluble sugar concentrations might influence the observed stability of total NSC concentrations along the Ψ_{PD} gradient observed during plant dehydration. In this context, it has been recently shown that the total amount of stored NSC is not very responsive to environmental stress across plants from various global biomes (Blumstein et al. 2022). However, starch concentrations did exhibit a strong early decline under decreasing Ψ_{PD}. Rapid exponential declines in starch reserves co-occurred in all 12 species measured. These findings are in line with a meta-analysis including 52 tree species and showing strong drought-induced starch decreases in

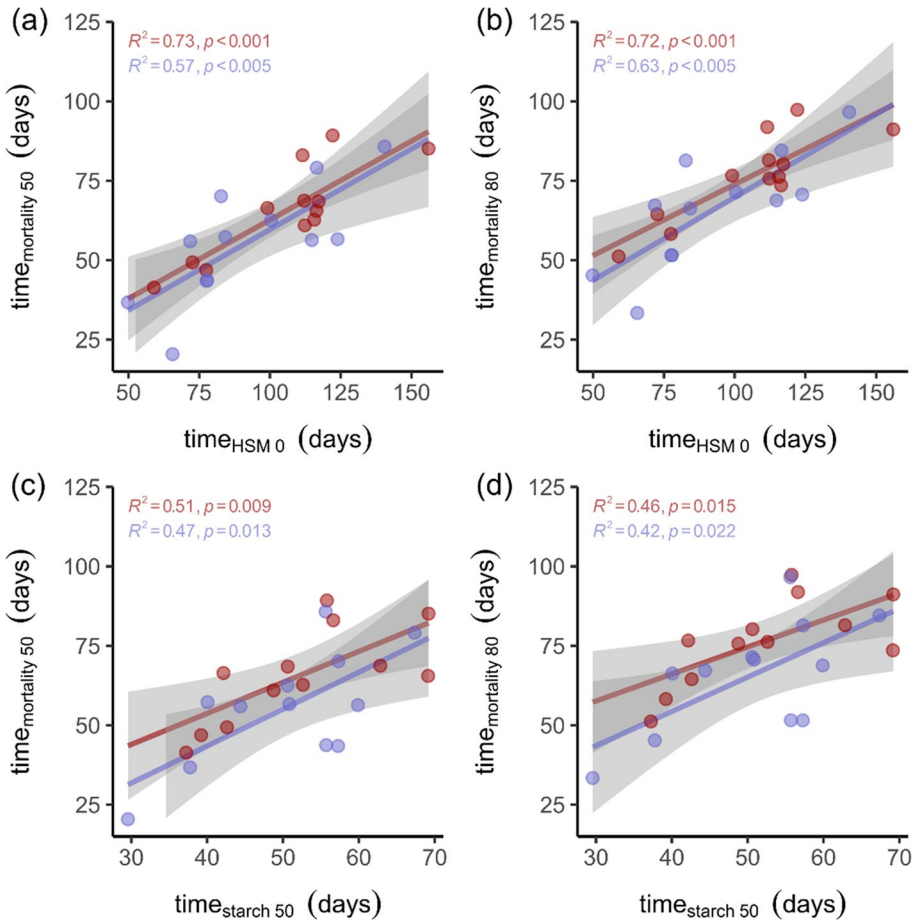

Fig. 9 Mortality thresholds are explained by the elapsed time to reach a null hydraulic safety margin and to deplete starch. Relationships between the time thresholds to reach 50% and 80% mortality and $time_{HSM0}$ (**a**, **b**), the time to reach a null safety margin (Ψ_{MD}—Ψ_{50}), along with $time_{starch50}$ (**c**, **d**), the time to consume 50% of total starch concentrations. Different colors in dots and regression lines correspond to light-exposed (blue) and shaded (red) individuals before the drought experiment. Strong correlations between mortality, starch depletion, and HSM times were also observed when pooling both treatments together (Appendix Table 8). PGLS regressions supporting these relationships are also available in Appendix Table 9

different plant organs, while soluble sugars showed less significant declines (He et al. 2020).

Starch is an insoluble glucan and it is the most preponderant storage carbohydrate in plants with important roles in growth and nocturnal respiration (Zeeman et al. 2010). In this study, we use a new metric, $time_{starch50}$, which is the time rate to consume half of the starch reserves in the plant, to accurately predict seedling mortality rates. It has been argued that under drought, starch is likely hydrolyzed early to contribute to maintain osmotic potential and to rapidly mitigate stress (He et al. 2020). Given the daily importance of starch to support metabolism during the night (Thalmann and Santelia 2017), our results suggest that plants under drought stress might suffer from a lack of transitory starch, which is essential to support plant metabolism. Further, the starch depletion trends that we observed suggest that plants might rely on soluble sugars for osmotic regulations, since the early drought onset (Thalmann and Santelia 2017; Hartmann et al. 2021). Starch remobilisation can also provide carbon skeletons for osmolytes such as proline (Muller et al. 2011). Further, under drought conditions, carbon-limited plants actively store NSC through gene upregulation as a priority over growth (Smith and Stitt 2007; Huang et al. 2021), which could explain the lack of biomass gain observed in our experiment. It has been suggested that such a need for sugars, including starch conversion to osmolytes to maintain the osmotic potential of living cells and a more negative turgor loss point, would be more relevant in species with a less strict stomatal control (Hartmann et al. 2021). Yet, the vast majority of the species studied here seemed to have partial stomatal control on water loss. The ubiquitous declines in starch across the studied species and

its relation to seedling mortality, suggest that regardless of the stomatal control under drought, starch depletion might play a role in early drought responses and help counteract partly the reduction in photosynthetic carbon uptake.

Our study also shows that most of the total NSC concentration was allocated to the leaves, followed by the stem and the roots, which had rather similar concentrations to one another. These findings are in accordance with a meta-analysis across 177 species from various biomes (Martínez-Vilalta et al. 2016), suggesting a prevalence for NSC to be allocated to (or retained in) leaves over other plant organs. Leaves retained the highest NSC reserves even after major drought stress in our experiment. Such differences in NSC concentrations among organs arise from the larger concentrations of soluble sugars in leaves compared to other organs, whilst starch amounts did not vary significantly amongst organs. It is remarkable that pre-drought starch concentrations were equal across organs since such carbohydrate reserves are frequently associated with storage organs such as roots and rhizomes (Thalmann and Santelia 2017). In a previous study analyzing partitioning of NSC concentrations across organs, roots showed even lower starch concentrations in comparison to leaves and stems (Furze et al. 2019). However, our study pinpoints that after severe drought, roots become the larger starch reserve in the plant. Our results, which clearly show that the time to consume starch concentrations is key in explaining mortality rates, highlight the importance of starch storage as a drought tolerance strategy in plants. In this line, a recent study analyzing xylem starch storage in a seasonally dry tropical forest has shown that tree species with higher starch pools have lower mortality rates (Herrera-Ramírez et al. 2021).

4.3 Light environments, the hydraulic safety margin and its importance in explaining plant mortality

Previous studies suggest that shaded, NSC-depleted individuals have higher xylem vulnerability under drought stress (Tomasella et al. 2021) and higher mortality rates (O'Brien et al. 2014). Interestingly, we found that individuals who were subject to high irradiance during the light manipulation phase reached mortality earlier than shaded individuals. Given that individuals from the two light treatments did not show clear differences in total NSC concentrations prior to the drought phase, our findings suggest that only partial carbohydrate consumption could explain seedling mortality and that hydraulic failure might play a concomitant role. Indeed, while total NSC levels remained stable, starch levels declined untimely, suggesting that mortality would be partially caused by hydraulic failure, partial carbon depletion, and their interaction (Adams et al. 2017). Although starch concentration decreased drastically in all species, such declines occurred before reaching very negative values of predawn water potentials, suggesting that starch depletion takes effect early in the dehydration process and even before reaching critical water potentials that could damage the hydraulic capacity of the plants. It is noteworthy that light-exposed individuals retained slightly higher above-ground biomasses under drought conditions, which could have implied marginally higher cumulative transpiration. This might also explain why light-exposed individuals reached higher mortality and a null hydraulic safety margin ($time_{HSM0}$) earlier than shaded individuals. Interestingly, *Quercus ilex*, the only species that showed earlier mortality on plants under the shade treatment, also had remarkably higher biomasses in shaded individuals at the beginning of the drought experiment. This result suggests that plants with higher biomass gains at the onset of drought, which might have been achieved through enhanced transpiration and starch consumption, had higher mortality rates.

The hydraulic trait Ψ_{50}, a commonly used threshold of hydraulic failure induced by drought stress, did not explain mortality alone. However, $time_{HSM0}$, the elapsed time to reach a null hydraulic safety margin (HSM), which combines measurements of Ψ_{50} but also of Ψ_{MD}, was a good predictor of plant mortality, which explained more variance than starch depletion. This is in accordance with a meta-analysis of 26 diverse species showing that hydraulic failure is a more ubiquitous driver of tree mortality when compared to NSC reserve depletion (Adams et al. 2017). Similarly, the slope of the relationship of HSM over time, which reflects the pace at which a plant reaches negative safety margins, was a good predictor of mortality probability in the studied species. The pace at which water potential drops and reaches the HSM is therefore central to plant survival during drought stress. The pace to reach the HSM might arise from important features that were not considered in this study such as g_{min}, the hydraulic conductance after stomatal closure (Duursma et al. 2019). Therefore, it would be interesting to combine traits related to water loss regulation such as g_{min} and the HSM to implement more refined metrics such as the stomatal safety margin that has been recently proposed as a good predictor of drought survival in conifers (Petek-Petrik et al. 2023).

Other thresholds of hydraulic failure such as Ψ_{88}, the xylem pressure inducing an 88% loss of hydraulic conductance, have been advanced as potential thresholds of lethal drought-induced dysfunction (Urli et al. 2013). Moreover, recent studies have shown that angiosperm and gymnosperm species can go beyond the commonly used hydraulic thresholds of Ψ_{88} and Ψ_{50} before reaching lethal hydraulic tensions (Hammond et al. 2019; Mantova

et al. 2021). Yet, our study shows that significant mortality percentages can be observed even before reaching the limits of the hydraulic safety margin based on Ψ_{MD}—Ψ_{50}. This might arise from the fact that Ψ_{50} values were calculated on branch samples from other individuals, along with potentially precocious mortality rates from our visual estimations. However, in all species, $time_{mortality50}$ occurred earlier than $time_{HSM0}$, indicating that important drought-induced seedling injuries can be reached prior to reaching negative safety margins. Our findings on the occurrence of plant mortality before reaching negative safety margins are particularly relevant under the current climate change context where many plant species that operate within narrow safety margins would experience higher drought mortality risk (Choat et al. 2012, 2018).

5 Conclusion

This study adds to a growing body of research showing that a wider HSM would lower mortality risk in various biomes from temperate and tropical latitudes (Anderegg et al. 2016; Powers et al. 2020; Li et al. 2020; Hajek et al. 2022; Morcillo et al. 2022). The rates of 50% starch depletion occurred earlier than equivalent mortality rates and were strongly correlated, providing an important metric to predict seedling mortality. Nonetheless, $time_{HSM0}$ was a stronger predictor of mortality rate. Combining new safety indicators depicting the interaction of HSM with hydraulic thresholds of other key plant functions such as turgor loss, stomatal control, and rehydration capacity (Bartlett et al. 2016; Trueba et al. 2019) might help to refine such hydraulic traits of drought sensitivity and to produce more timely predictors. Ultimately, our study underlines that mortality results from the combined effects of early starch consumption followed by hydraulic dysfunction. Further efforts to carry out large-scale manipulation experiments like the one presented here, combined with in situ measurements of plant starch levels and water status during peaks of drought stress, will allow filling important gaps to understand the underlying mechanisms driving plant mortality and to improve forest dieback predictions.

Appendix

Table 2 Comparisons of plant total NSC (mg g^{-1} DW_{plant}) between light-exposed and shaded treatments measured at harvest 2, prior to the drought phase

Species	Light	Shade	*F*	DF	*p*
Abies nordmanniana	49.37	33.66	5.398	6	**0.05**
Arbutus unedo	25.55	26.63	0.022	7	0.886
Buxus sempervirens	59.77	62.04	0.155	6	0.707
Cedrus atlantica	12.68	9.33	0.992	6	0.358
Cupressus macrocarpa	18.14	30.16	6.311	6	**0.046**
Ilex aquifolium	55.30	39.49	14.304	6	**0.009**
Juniperus thurifera	35.03	31.15	0.342	6	0.58
Pinus halepensis	12.83	9.16	8.678	6	**0.026**
Pinus pinaster	33.79	30.99	0.142	6	0.719
Pinus sylvestris	28.39	26.36	0.194	6	0.675
Quercus ilex	23.90	23.25	0.018	6	0.897
Tetraclinis articulata	12.26	12.52	0.014	6	0.911

Average total NSC concentrations (in mg g^{-1}) per species and treatments are provided. Statistics of independent measures ANOVA are included. *F* values, degrees of freedom, and *p* values for the treatment comparisons are provided. Significant differences between treatments at $\alpha = 0.05$ are highlighted in bold

Table 3 Analysis of variance of plant total NSC concentrations (mg g^{-1} DW_{plant}) as a function of light treatments and species, including the interaction between both terms

Fixed effects	Sum of squares	Mean square	*F*	DF	*p*
Light treatment	179	179	3.11	1	0.08
Species	20,229	1839	32.07	11	**≤ 0.001**
Light treatment: Species	1229	112	1.95	11	**0.04**

Analyses were carried out on total NSC concentrations immediately after the light manipulation phase and before the drought phase. Significant effects at $\alpha = 0.05$ are highlighted in bold

Table 4 Comparisons of total NSC in three different plant organs between different irradiance treatments before the drought phase

Species	Leaf				Stem				Root			
	Mean	*F*	DF	*p*	Mean	*F*	DF	*p*	Mean	*F*	DF	*p*
Abies nordmanniana	36.14	1.911	6	0.216	25.97	10.574	5	**0.023**	25.94	1.014	6	0.353
Arbutus unedo	23.08	1.073	7	0.335	31.82	10.459	7	**0.014**	30.13	0.06	7	0.813
Buxus sempervirens	60.95	0.316	6	0.594	41.03	6.226	6	**0.047**	43.57	0.039	6	0.85
Cedrus atlantica	15.51	0.648	6	0.451	16.26	3.312	6	0.119	5.45	2.657	6	0.154
Cupressus macrocarpa	23.38	8.582	6	**0.026**	11.46	0.41	6	0.546	11.64	1.592	6	0.254
Ilex aquifolium	64.30	2.489	6	0.166	42.19	5.477	6	0.058	43.41	6.605	6	**0.042**
Juniperus thurifera	33.67	0.065	6	0.808	19.43	0.034	6	0.86	12.54	2.928	6	0.138
Pinus halepensis	23.51	0.09	6	0.774	19.80	5.179	6	0.063	12.75	2.498	6	0.165
Pinus pinaster	33.83	0.064	6	0.809	28.48	0.116	6	0.745	15.92	3.624	6	0.106
Pinus sylvestris	39.30	0.66	6	0.448	33.67	0.417	6	0.542	18.31	2.007	6	0.206
Quercus ilex	36.20	0.748	6	0.42	24.01	18.761	6	**0.005**	27.24	0.19	6	0.678
Tetraclinis articulata	13.68	0.805	6	0.404	19.28	3.317	6	0.118	10.76	0.023	6	0.885

Total NSC (mg g^{-1} DW_{organ}) in light-exposed and shaded treatments were measured at harvest 2, before the drought phase (see the "Materials and Methods" section for details). Statistics of independent measures ANOVA are included. Means, *F* values, degrees of freedom, and *p* values for the treatment comparisons are provided. Significant differences between treatments at $\alpha = 0.05$ are highlighted in bold

Table 5 Thresholds of time at different percentages of mortality

Species	Treatment	*a*	*b*	X_o	R^2	AICc	$Time_{mortality10\%}$	$Time_{mortality50\%}$	$Time_{mortality80\%}$
Abies nordmanniana	Shaded	99.87	0.99	5.90	0.83	4997.16	3.68	5.91	7.31
Abies nordmanniana	Light-exposed	100.03	1.14	5.25	0.83	5089.48	3.33	5.25	6.46
Arbutus unedo	Shaded	101.07	0.84	6.73	0.86	4871.01	4.09	6.70	8.32
Arbutus unedo	Light-exposed	100.41	0.74	2.93	0.65	6679.14	-0.04	2.92	4.77
Buxus sempervirens	Shaded	101.02	0.93	9.51	0.86	6061.82	7.12	9.49	10.95
Buxus sempervirens	Light-exposed	99.50	1.09	8.17	0.86	5847.37	6.16	8.18	9.47
Cedrus atlantica	Shaded	101.36	0.64	8.75	0.75	3685.96	5.30	8.71	10.81
Cedrus atlantica	Light-exposed	99.98	1.20	6.21	0.85	5818.86	4.38	6.21	7.36
Cupressus macrocarpa	Shaded	101.04	0.81	9.81	0.81	6473.27	7.08	9.78	11.46
Cupressus macrocarpa	Light-exposed	99.74	1.25	6.25	0.86	5430.73	4.49	6.25	7.37
Ilex aquifolium	Shaded	101.30	0.70	9.00	0.78	6346.88	5.84	8.96	10.89
Ilex aquifolium	Light-exposed	100.38	0.69	8.10	0.77	6007.26	4.89	8.09	10.09
Juniperus thurifera	Shaded	98.16	1.25	12.72	0.91	5190.16	10.98	12.75	13.90
Juniperus thurifera	Light-exposed	93.85	1.05	12.13	0.80	6057.17	10.10	12.25	13.80
Pinus halepensis	Shaded	99.94	1.21	9.36	0.87	5855.02	7.54	9.36	10.51
Pinus halepensis	Light-exposed	99.97	1.09	8.93	0.86	5871.42	6.92	8.93	10.20
Pinus pinaster	Shaded	100.06	1.61	12.16	0.91	5200.37	10.80	12.16	13.02
Pinus pinaster	Light-exposed	100.32	1.78	11.31	0.92	5856.46	10.07	11.30	12.08
Pinus sylvestris	Shaded	100.11	1.09	11.86	0.84	5256.10	9.84	11.86	13.13
Pinus sylvestris	Light-exposed	101.72	0.84	10.06	0.83	5842.49	7.41	10.02	11.62
Quercus ilex	Shaded	99.99	0.64	7.05	0.71	4824.90	3.62	7.05	9.21
Quercus ilex	Light-exposed	100.32	0.85	7.99	0.82	4774.35	5.41	7.99	9.60
Tetraclinis articulata	Shaded	101.53	0.74	9.86	0.80	5583.37	6.86	9.82	11.64
Tetraclinis articulata	Light-exposed	100.22	0.77	8.05	0.78	5247.28	5.20	8.05	9.83

Coefficients of determination, AICc, and parameter estimates of logistic fits are provided. Time thresholds (in weeks) of shaded and light-exposed treatments for each species are included

Table 6 Thresholds of elapsed time to reach a null hydraulic safety margin

Species	Treatment	*a*	*b*	R^2	AICc	$Time_{HSM\,0}$
Abies nordmanniana	Shaded	3.70	−0.38	0.46	105.26	59.01
Abies nordmanniana	Light-exposed	5.50	−0.78	0.64	121.75	49.84
Arbutus unedo	Shaded	10.28	−0.83	0.80	117.62	77.49
Arbutus unedo	Light-exposed	8.53	−0.88	0.91	92.42	65.59
Buxus sempervirens	Shaded	9.69	−0.68	0.73	115.56	99.12
Buxus sempervirens	Light-exposed	10.43	−0.87	0.86	96.58	84.28
Cedrus atlantica	Shaded	5.04	−0.25	0.69	67.02	112.28
Cedrus atlantica	Light-exposed	5.48	−0.39	0.52	111.13	77.63
Cupressus macrocarpa	Shaded	7.66	−0.33	0.57	87.33	117.18
Cupressus macrocarpa	Light-exposed	9.58	−0.77	0.72	130.56	77.84
Ilex aquifolium	Shaded	8.17	−0.49	0.57	128.06	115.64
Ilex aquifolium	Light-exposed	8.07	−0.46	0.57	128.39	123.9
Juniperus thurifera	Shaded	10.82	−0.50	0.69	121.58	122.15
Juniperus thurifera	Light-exposed	10.54	−0.41	0.68	108.71	140.49
Pinus halepensis	Shaded	5.09	−0.26	0.77	42.77	116.41
Pinus halepensis	Light-exposed	5.00	−0.31	0.81	42.81	100.45
Pinus pinaster	Shaded	3.34	−0.11	0.67	22.79	156.03
Pinus pinaster	Light-exposed	3.76	−0.20	0.82	39.92	116.55
Pinus sylvestris	Shaded	3.11	−0.14	0.59	56.62	111.51
Pinus sylvestris	Light-exposed	3.57	−0.26	0.69	62.93	82.74
Quercus ilex	Shaded	8.15	−0.64	0.57	126.15	72.66
Quercus ilex	Light-exposed	9.30	−0.82	0.73	104.43	71.82
Tetraclinis articulata	Shaded	15.96	−0.88	0.80	114.92	112.07
Tetraclinis articulata	Light-exposed	15.19	−0.87	0.89	99.54	114.8

Coefficients of determination, AICc, and parameter estimates of linear fits are provided. Time thresholds (in days) of shaded and light-exposed treatments for each species are included

Table 7 Thresholds of elapsed time to deplete 50% of starch concentration

Species	Treatment	*a*	*b*	R^2	AICc	$Time_{starch50\%}$
Abies nordmanniana	Shaded	53.87	−0.72	0.59	150.37	37.23
Abies nordmanniana	Light-exposed	57.87	−0.77	0.59	152.74	37.74
Arbutus unedo	Shaded	16.83	−0.21	0.33	127.15	39.21
Arbutus unedo	Light-exposed	20.59	−0.35	0.51	113.93	29.55
Buxus sempervirens	Shaded	92.70	−1.10	0.92	130.92	42.15
Buxus sempervirens	Light-exposed	91.41	−1.14	0.88	131.53	40.04
Cedrus atlantica	Shaded	10.88	−0.11	0.68	81.33	48.75
Cedrus atlantica	Light-exposed	8.19	−0.07	0.39	82.33	57.26
Cupressus macrocarpa	Shaded	12.24	−0.12	0.71	86.34	50.62
Cupressus macrocarpa	Light-exposed	6.64	−0.06	0.71	61.92	55.68
Ilex aquifolium	Shaded	8.55	−0.08	0.48	94.05	52.62
Ilex aquifolium	Light-exposed	15.35	−0.15	0.51	110.16	50.83
Juniperus thurifera	Shaded	30.69	−0.28	0.88	97.06	55.78
Juniperus thurifera	Light-exposed	30.36	−0.27	0.77	102.51	55.61
Pinus halepensis	Shaded	12.68	−0.09	0.63	82.90	69.13
Pinus halepensis	Light-exposed	13.33	−0.13	0.73	81.21	50.58
Pinus pinaster	Shaded	20.40	−0.15	0.57	97.94	69.19
Pinus pinaster	Light-exposed	25.26	−0.19	0.30	136.20	67.35
Pinus sylvestris	Shaded	11.24	−0.10	0.85	72.43	56.62
Pinus sylvestris	Light-exposed	10.39	−0.09	0.79	66.68	57.30
Quercus ilex	Shaded	39.20	−0.46	0.71	134.22	42.61
Quercus ilex	Light-exposed	42.11	−0.47	0.67	109.75	44.38
Tetraclinis articulata	Shaded	19.75	−0.16	0.49	107.94	62.83
Tetraclinis articulata	Light-exposed	15.55	−0.13	0.61	94.66	59.88

Coefficients of determination, AICc, and parameter estimates of linear fits are provided. Time thresholds (in days) of shaded and light-exposed treatments for each species are included

Table 8 Plant mortality thresholds as explained by hydraulic safety margin features and starch depletion

	$Time_{mortality\ 10\%}$				$Time_{mortality\ 50\%}$				$Time_{mortality\ 80\%}$			
	Intercept	**Slope**	R^2	***p* value**	**Intercept**	**Slope**	R^2	***p* value**	**Intercept**	**Slope**	R^2	***p* value**
$Time_{HSD\ 0}$	−0.14	0.39	0.63	**< 0.001**	2.62	0.37	0.68	**< 0.001**	4.31	0.35	0.68	**< 0.001**
$Slope_{HSD\sim time}$	9.42	6.00	0.34	**< 0.01**	11.39	5.23	0.32	**< 0.01**	12.64	4.76	0.29	**< 0.05**
$Time_{starch\ 50\%}$	−20.65	1.26	0.50	**< 0.001**	4.19	1.09	0.47	**< 0.001**	19.83	0.99	0.42	**< 0.001**

Analysis performed on pooled data combining both light treatments. Linear regression statistics are included and significant relations at $\alpha = 0.05$ are indicated in bold

Table 9 Phylogenetically corrected relationships between plant mortality thresholds, hydraulic safety margin features, and starch depletion

	$Time_{mortality\ 10\%}$					$Time_{mortality\ 50\%}$					$Time_{mortality\ 80\%}$				
	Intercept	**Slope**	R^2	***p* value**	**λ**	**Intercept**	**Slope**	R^2	***p* value**	**λ**	**Intercept**	**Slope**	R^2	***p* value**	**λ**
$Time_{HSD\ 0}$	−1.55	0.47	0.75	**< 0.001**	0.00	1.68	0.42	0.77	**< 0.001**	0.00	3.66	0.39	0.75	**< 0.001**	0.00
$Slope_{HSD\sim time}$	9.64	6.42	0.38	**< 0.05**	0.00	11.36	5.17	0.32	0.054	0.00	12.46	4.41	0.26	0.09	0.00
$Time_{starch\ 50\%}$	−25.27	1.35	0.59	**< 0.005**	0.00	−1.33	1.21	0.60	**< 0.005**	0.00	13.71	1.12	0.58	**< 0.005**	0.00

Analysis performed on pooled data combining both light treatments. Phylogenetic generalized least squares (PGLS) statistics are included and significant relations at $\alpha = 0.05$ are indicated in bold

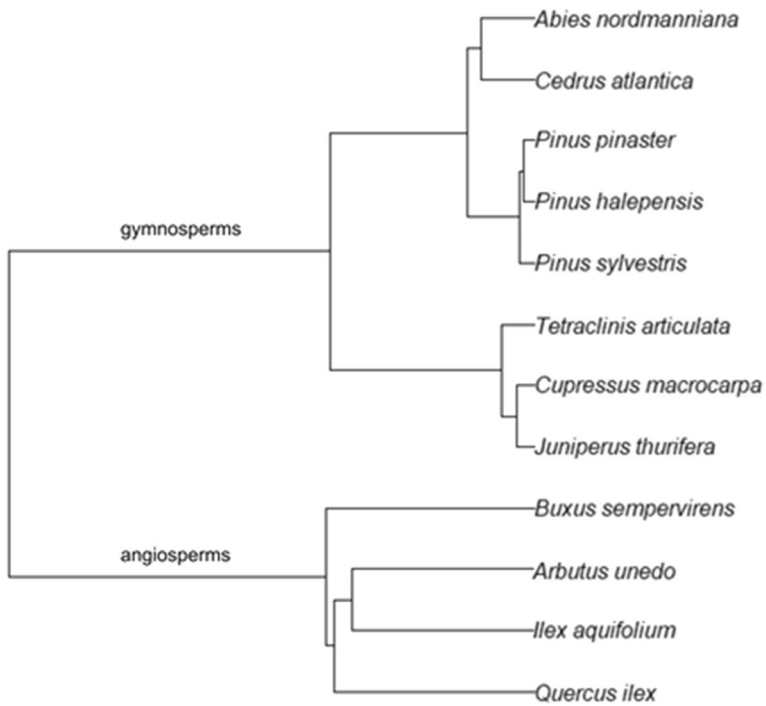

Fig. 10 Phylogenetic relationships across the 12 studied species. Labels in branches correspond to different clades

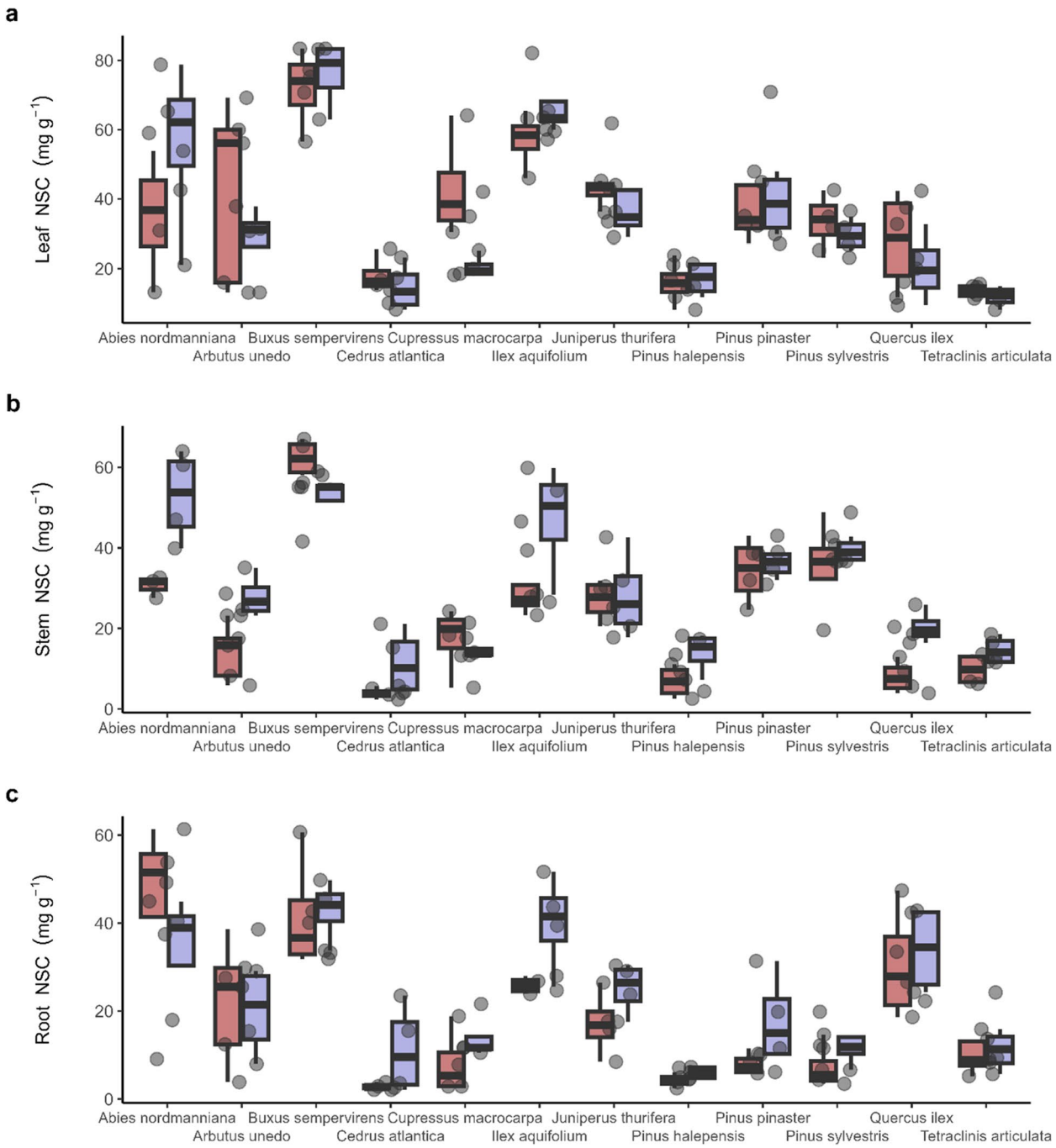

Fig. 11 Comparisons of total non-structural carbohydrate (NSC) concentrations in three different organs for 12 studied angiosperm and conifer species after the light manipulation phase and before the drought treatment. Light-exposed (blue) and shaded (red) individuals of each species are shown. Boxes and bars show the median, quartiles, and extreme values. Dots are individual data points. Significant differences between light treatments are indicated: *$p \leq 0.05$; **$p \leq 0.01$. See Appendix Tables 2, 3 and 4 for additional statistics comparing NSC levels of different light treatments and across plant organs

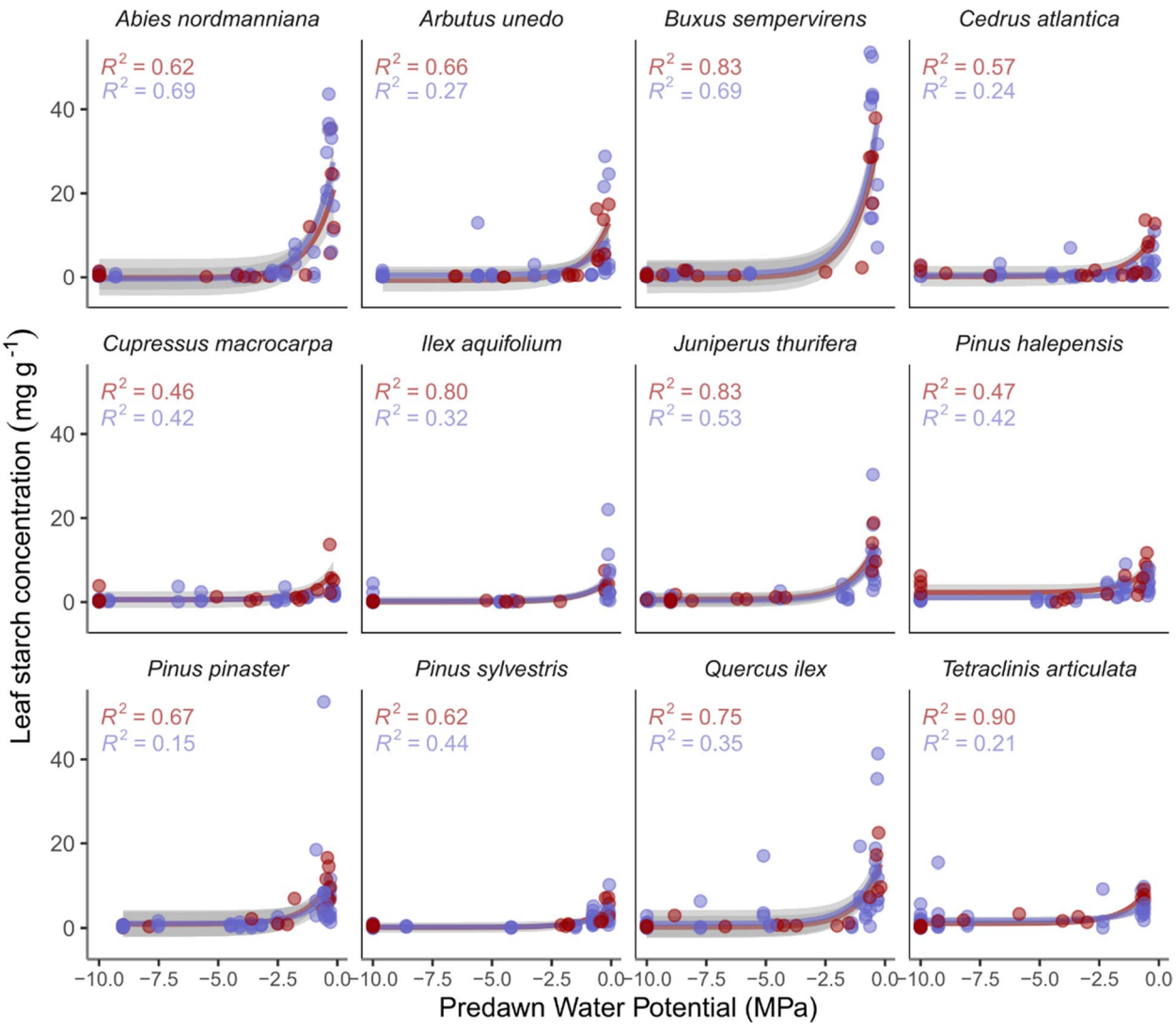

Fig. 12 Leaf starch concentration as a function of predawn water potential. Different colors in dots and lines correspond to light-exposed (blue) and shaded (red) individuals before the drought experiment. Solid regression lines, 95% confidence intervals (gray-shaded areas), and coefficients of determination are included

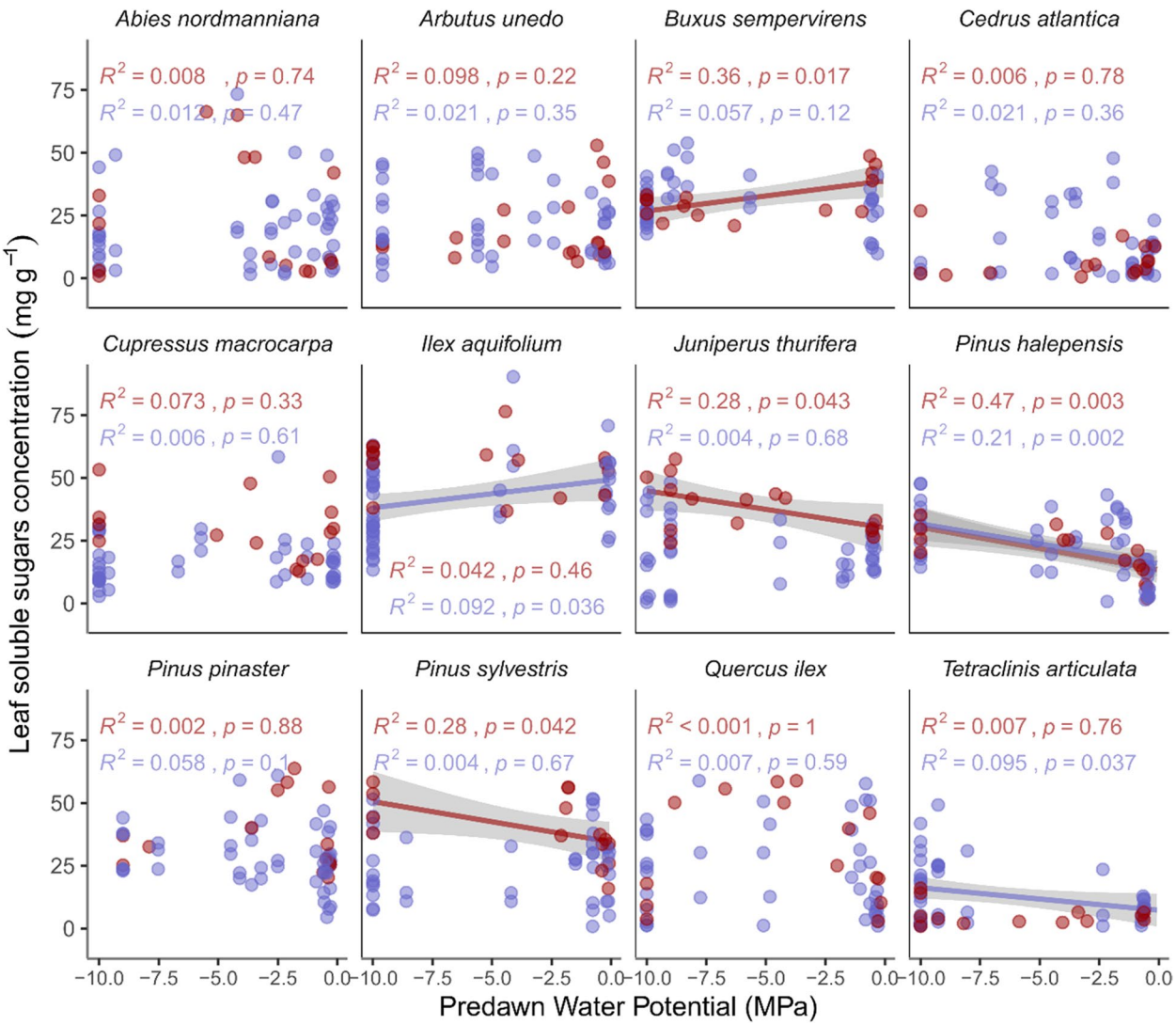

Fig. 13 Leaf soluble sugar concentration as a function of predawn water potential. Different colors in dots and lines correspond to light-exposed (blue) and shaded (red) individuals before the drought experiment. Solid regression lines and 95% confidence intervals (gray-shaded areas) depict significant relationships

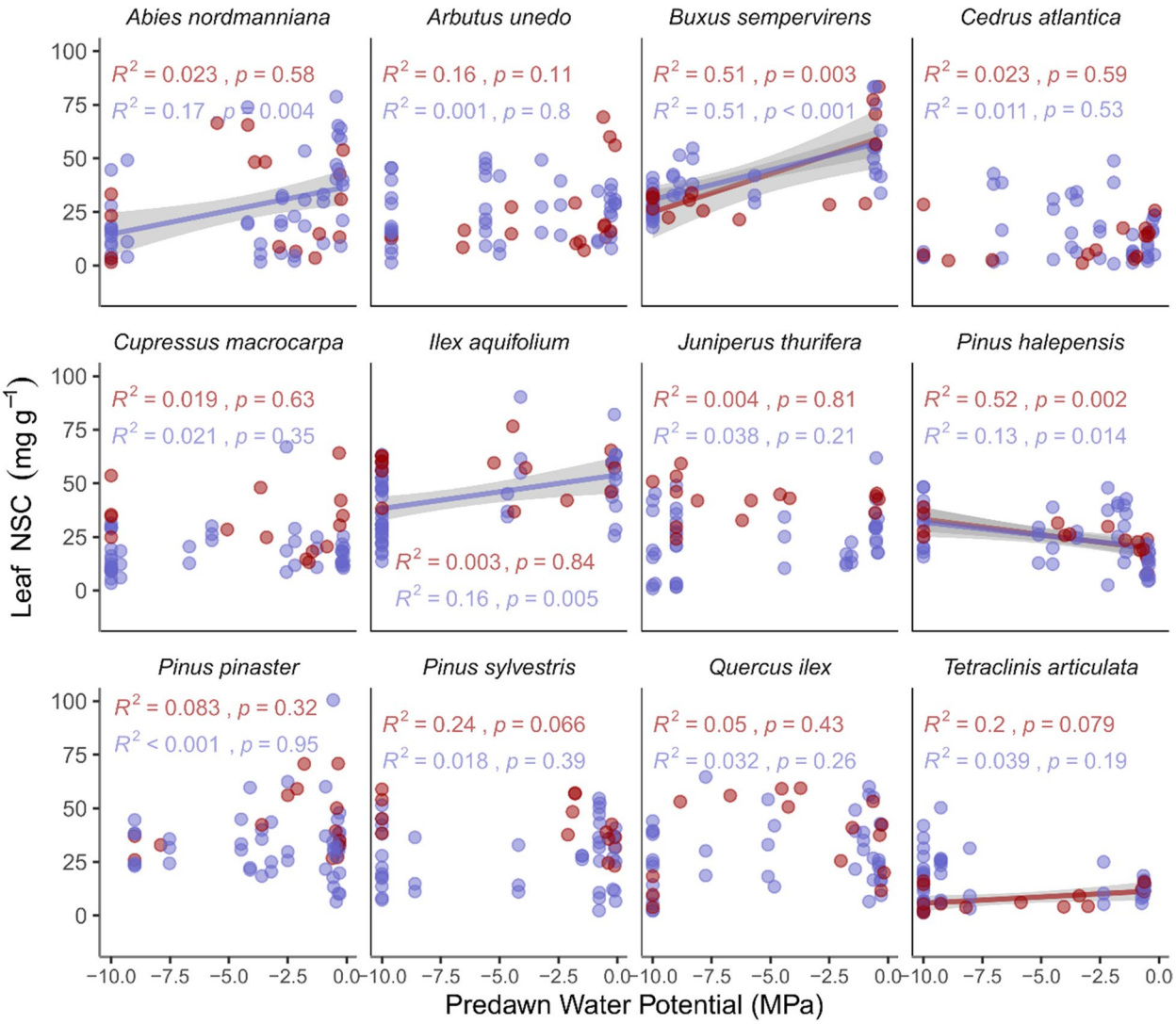

Fig. 14 Leaf total nonstructural carbohydrate concentrations as a function of predawn water potential. Different colors in dots and lines correspond to light-exposed (blue) and shaded (red) individuals before the drought experiment. Solid regression lines and 95% confidence intervals (gray-shaded areas) depict significant relationships. Coefficients of determination and *p* values are included for each light treatment

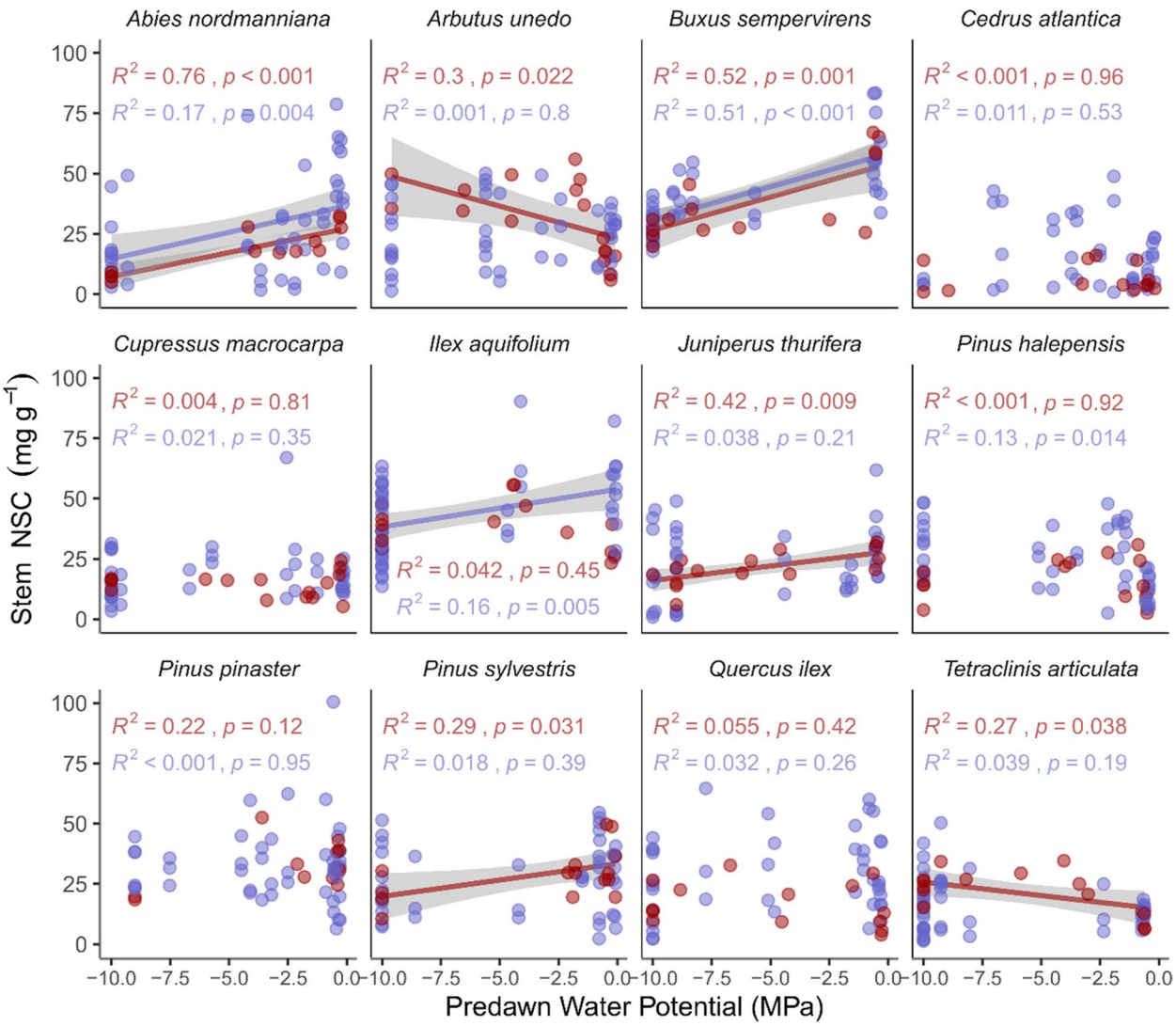

Fig. 15 Stem total nonstructural carbohydrate concentrations as a function of predawn water potential. Different colors in dots and lines correspond to light-exposed (blue) and shaded (red) individuals before the drought experiment. Solid regression lines and 95% confidence intervals (gray-shaded areas) depict significant relationships. Coefficients of determination and *p* values are included for each light treatment

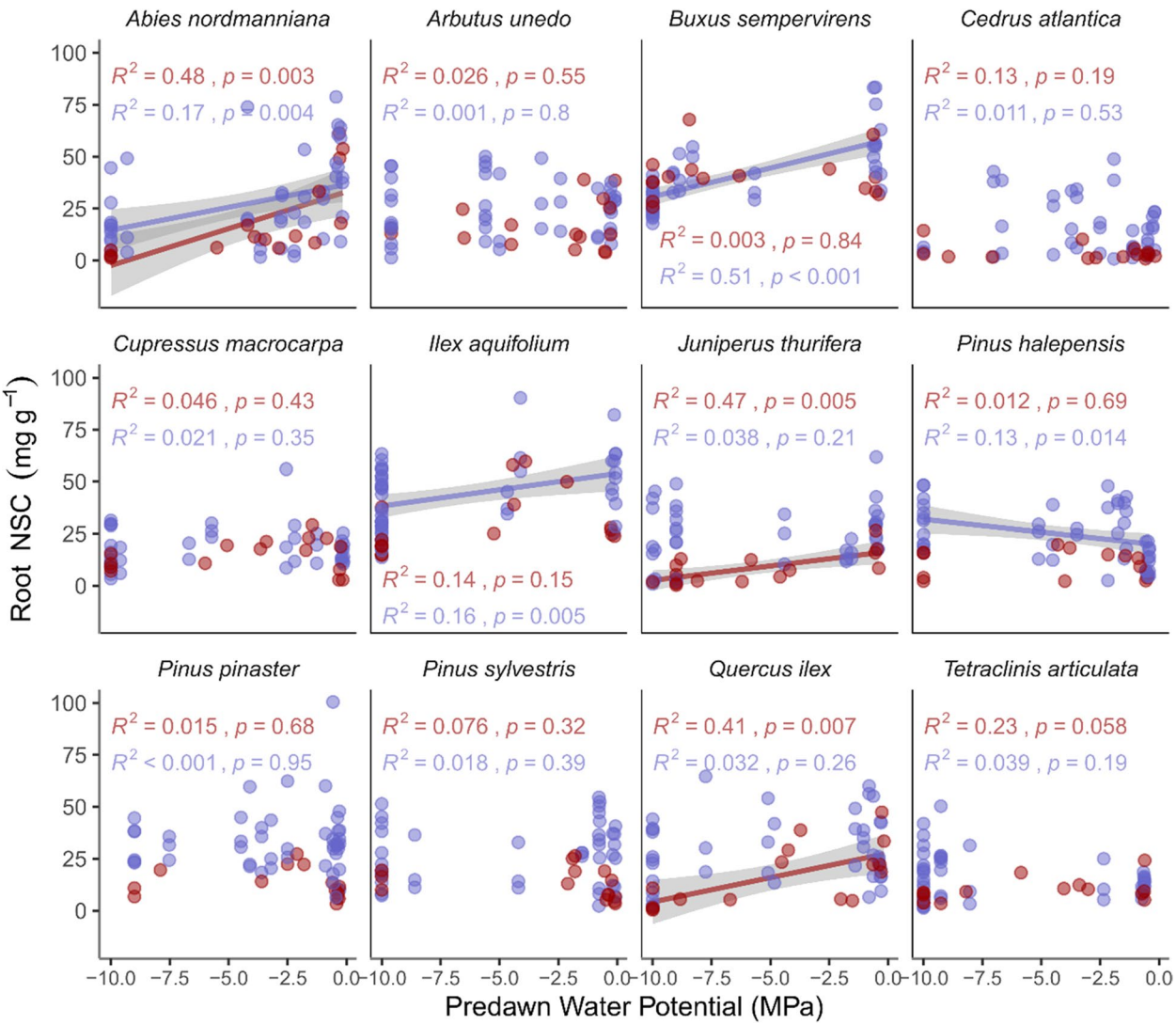

Fig. 16 Root total nonstructural carbohydrate concentrations as a function of predawn water potential. Different colors in dots and lines correspond to light-exposed (blue) and shaded (red) individuals before the drought experiment. Solid regression lines and 95% confidence intervals (gray-shaded areas) depict significant relationships. Coefficients of determination and *p* values are included for each light treatment

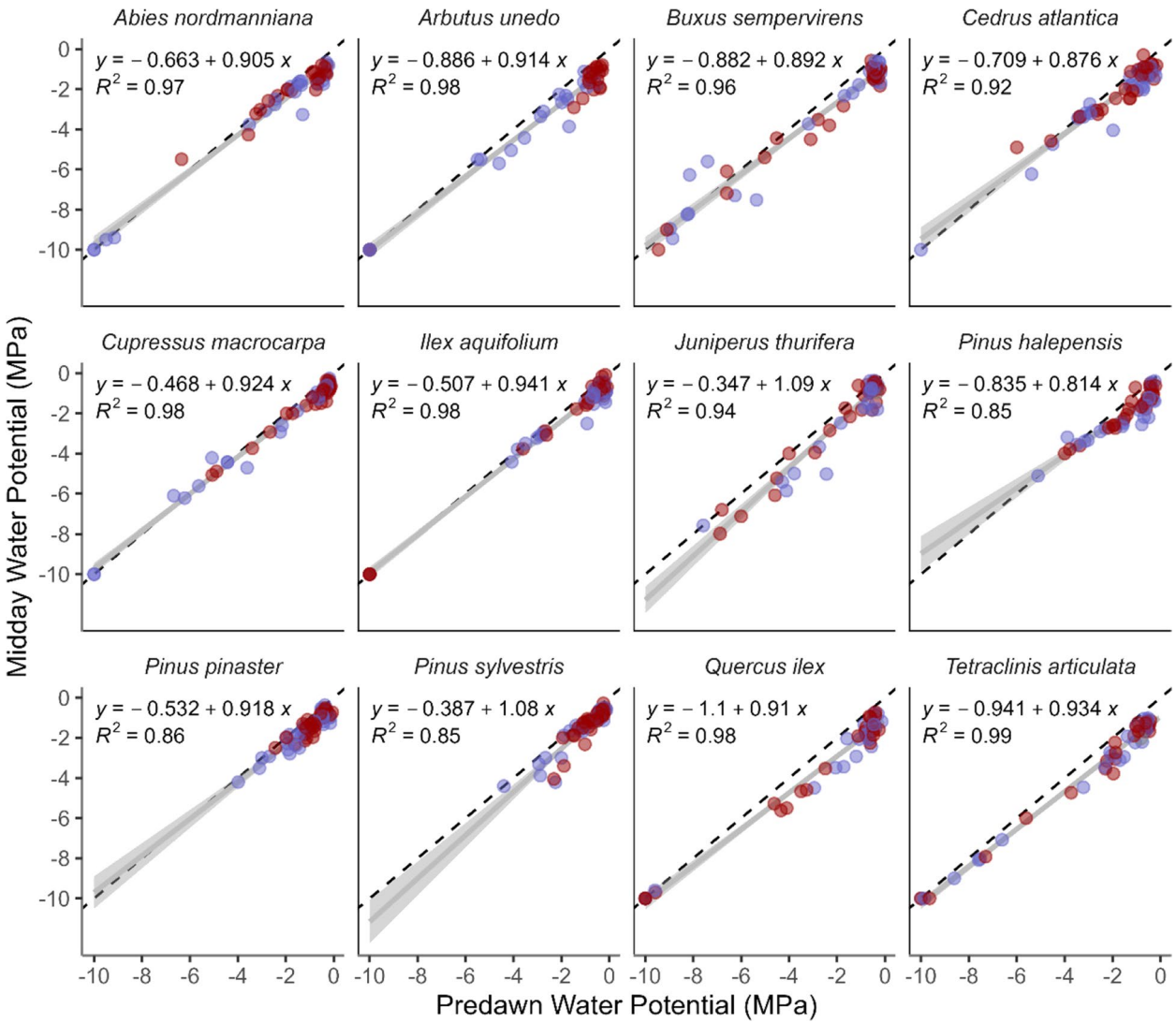

Fig. 17 Relationships between predawn and midday water potentials across 12 studied species. Points represent measurements carried out over the entire dehydration experiment, and different colors denote light-exposed (blue) and shaded (red) treatments. Solid regression lines and 95% confidence intervals (gray lines and shaded areas) are included. The 1:1 relationship is indicated by the black dashed line. Intercepts and slopes from linear regressions along with coefficients of determination for each species are provided

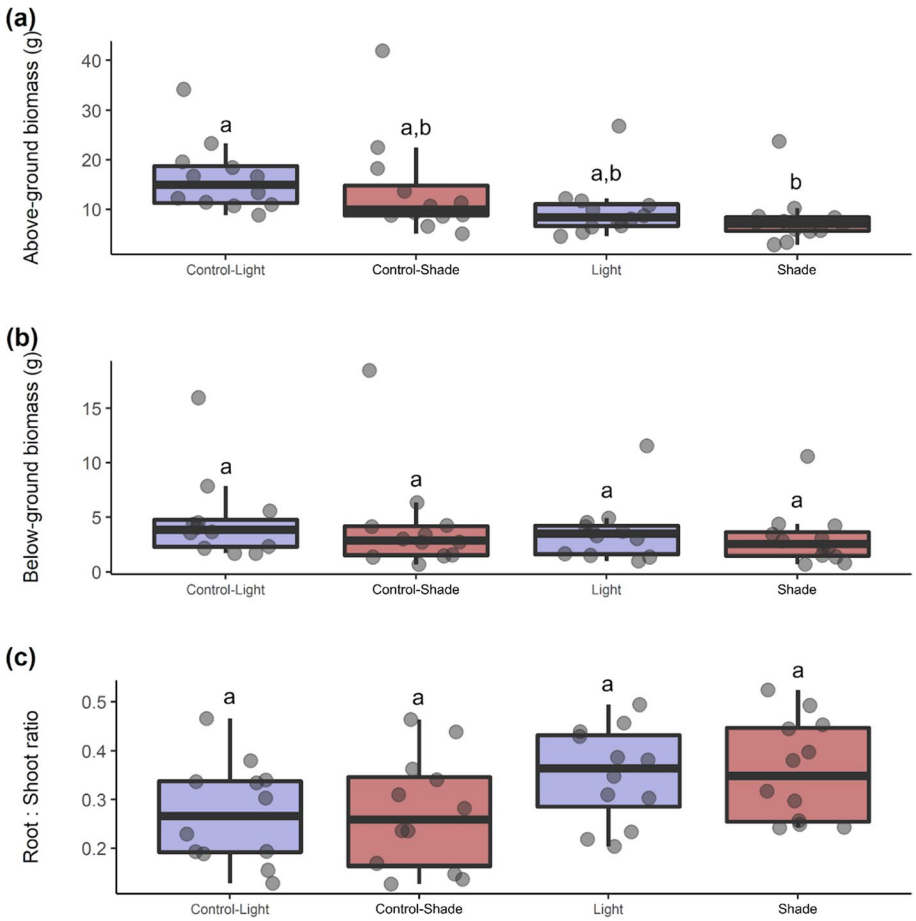

Fig. 18 Comparisons of biomass allocation for individuals growing under different light manipulation treatments and control individuals. Light-exposed (blue) and shaded (red) individuals of each species under severe drought stress (harvest 5) are shown, as well as their corresponding controls (watered individuals). Boxes and bars show the median, quartiles, and extreme values. Dots are individual data points. Letters indicate significant differences in biomass allocation across treatments

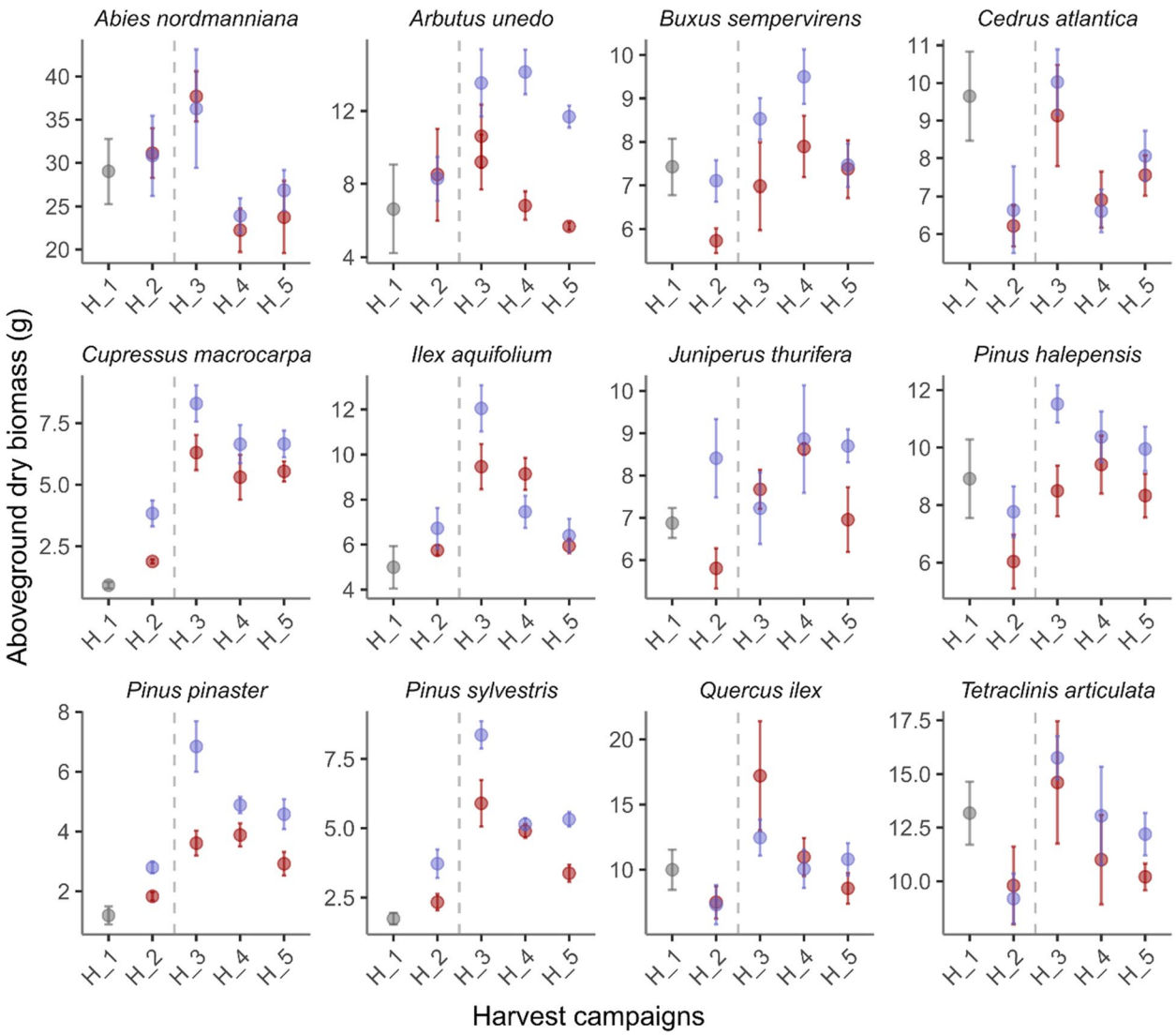

Fig. 19 Dynamics of aboveground dry biomass allocation for individuals growing under different light manipulation treatments. Light-exposed (blue) and shaded (red) individuals of each species at five different harvest campaigns (H_1 to H_5) are shown. *y* dots indicate aboveground dry biomass at harvest 1 (H_1), before the light manipulation treatment. The onset of drought is indicated with a dashed vertical line. Dots indicate mean aboveground dry biomass values and bars show the standard error. See the "Materials and Methods" section and Fig. 1 of the main text for a description of each harvest campaign

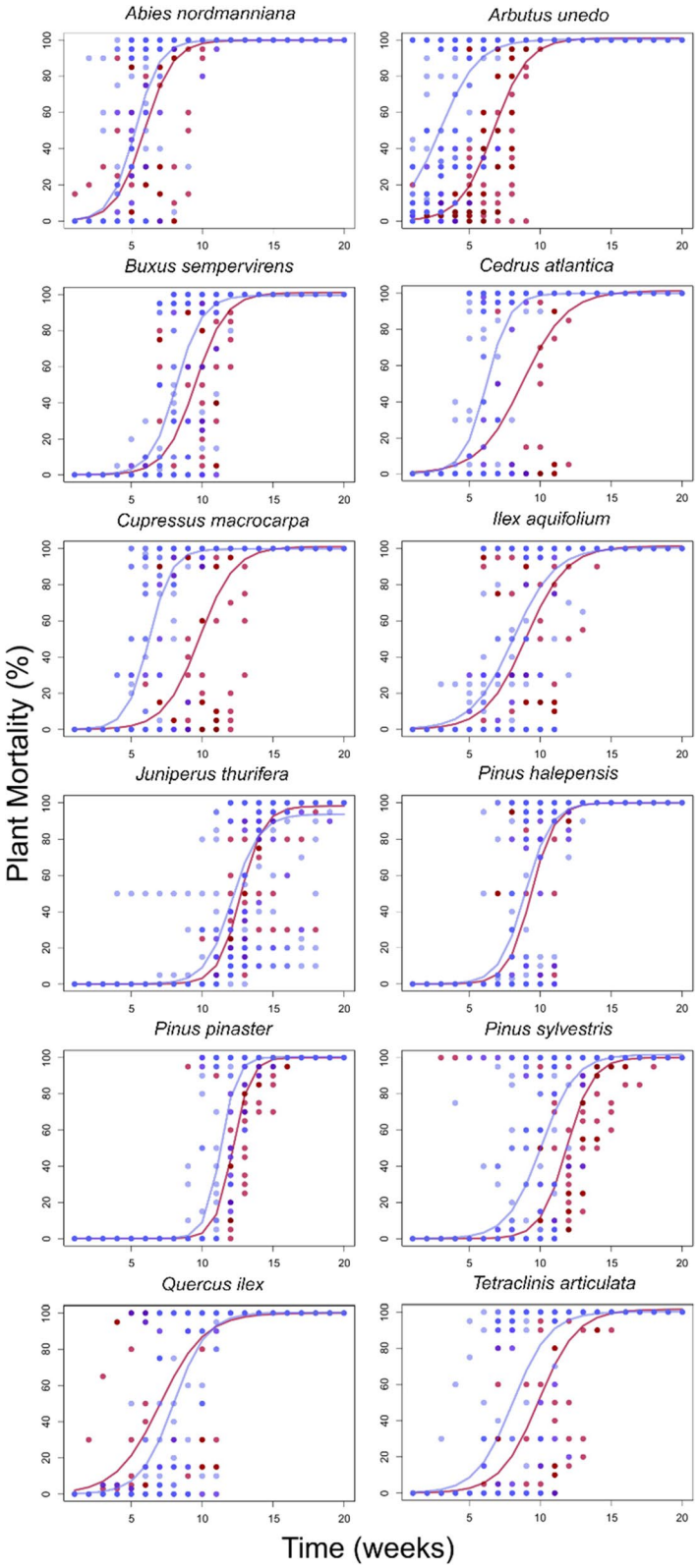

Fig. 20 Plant mortality as a function of time under drought conditions of 12 species following two different light irradiance treatments. Light-exposed (blue) and shaded (red) individuals of each species are distinguished. Curves are logistic regressions fitted for each light treatment. Model parameters and outputs are provided in Appendix Table 5

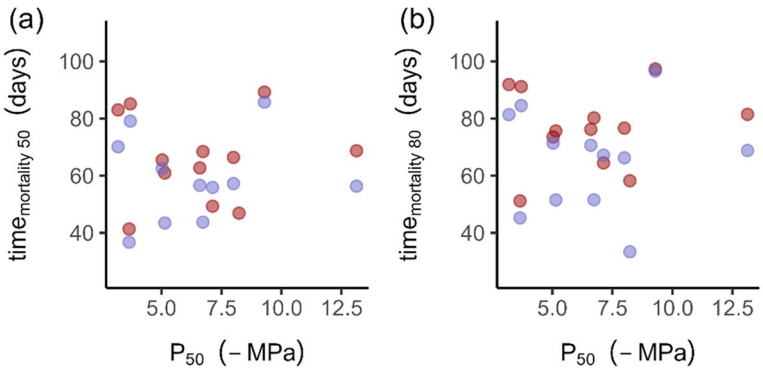

Fig. 21 Time at 50% and 80% mortality as a function of P_{50}, the water potential inducing 50% of loss in hydraulic conductivity. Dots represent species, different colors correspond to the light (blue) and shade (red) treatments before the drought experiment. We observe a lack of relationship between hydraulic failure and mortality time in both relationships presented in panel a ($r = -0.02$; $P = 0.93$) and b ($r = 0.05$; $P = 0.83$). A similar lack of relationships was observed when considering irradiance treatments independently (not shown)

Acknowledgements
We thank Gaëlle Capdeville, Deborah Corso, Jules Dellestable, Dean Sarger, Thomas Caignard, Marta Benito, Hafiz Bashir Ahmad, Thibaut Fréjaville, Bastien Fréjaville, Noelia Saavedra, and Jason West for kind assistance during the experimental period.

Reference to pre-print servers
Not applicable.

Authors' contributions
NGM, RB, and SD designed the study; NGM, RB, LJB, TEG, AK, CB, CL, JMT-R, LW, SD, and YG carried out the experiments and processed the samples; ST analyzed the data and wrote the first version of the manuscript; all coauthors contributed with manuscript revisions and approved the submitted version of the manuscript. The authors read and approved the final manuscript.

Funding
This study received financial support from the French government in the framework of the IdEX Bordeaux University "Investments for the Future" program/GPR Bordeaux Plant Sciences. Financial support from PHENOME (ANR-11-INBS-0012) is also acknowledged. ST was supported by an IdEx post-doctoral fellowship from the University of Bordeaux. NGM received support from the Agreenskills + fellowship program, which has received funding from the EU's Seventh Framework Program under grant agreement No. FP7-26719 (Agreenskills + contract). TEG received funding from the Spanish Ministry of Science (grant number: PID2019-107817RB-I00).

Availability of data and materials
All data supporting the findings of this study are available within the paper and its supplementary data are published online. Raw datasets are available here: https://doi.org/https://doi.org/10.57745/URI8QC.

Declarations

Ethics approval and consent to participate
Not applicable.

Consent for publication
All authors gave their informed consent to this publication and its content.

Competing interests
The authors declare that they have no competing interests.

Author details
[1]University of Bordeaux, INRAE, UMR BIOGECO, 33615 Pessac, France. [2]AMAP, University of Montpellier, CIRAD, CNRS, INRAE, IRD, Montpellier, France. [3]IES Francisco de Goya-La Elipa, Madrid, Spain. [4]Département Des Sciences de L'Environnement, Université du Québec à Trois-Rivières, Trois-Rivières, QC, Canada. [5]University of Bordeaux, INRAE, UMR BFP, 33883 Villenave d'Ornon, France. [6]INRAE, UMR ISPA, Villenave d'Ornon 33883, France. [7]CREAF, 08193 Bellaterra (Cerdanyola del Vallès), Catalonia, Spain. [8]Instituto de Recursos Naturales y Agrobiología (IRNAS), Consejo Superior de Investigaciones Científicas (CSIC), Seville 41012, Spain.

Received: 20 October 2023 Accepted: 8 July 2024
Published online: 02 August 2024

References

Adams HD, Zeppel MJ, Anderegg WR et al (2017) A multi-species synthesis of physiological mechanisms in drought-induced tree mortality. Nature Ecology & Evolution 1:1285

Anderegg WRL, Hicke JA, Fisher RA et al (2015b) Tree mortality from drought, insects, and their interactions in a changing climate. New Phytol 208:674–683. https://doi.org/10.1111/nph.13477

Anderegg WRL, Klein T, Bartlett M et al (2016) Meta-analysis reveals that hydraulic traits explain cross-species patterns of drought-induced tree mortality across the globe. Proc Natl Acad Sci. https://doi.org/10.1073/pnas.1525678113

Anderegg WRL, Flint A, Huang C, et al (2015a) Tree mortality predicted from drought-induced vascular damage. Nature Geosci 8:367–371. https://doi.org/10.1038/ngeo2400 http://www.nature.com/ngeo/journal/v8/n5/abs/ngeo2400.html#supplementary-information

Bartlett MK, Klein T, Jansen S et al (2016) The correlations and sequence of plant stomatal, hydraulic, and wilting responses to drought. Proc Natl Acad Sci 113:13098–13103. https://doi.org/10.1073/pnas.1604088113

Benito Garzón M, González Muñoz N, Wigneron J-P et al (2018) The legacy of water deficit on populations having experienced negative hydraulic safety margin. Glob Ecol Biogeogr 27:346–356. https://doi.org/10.1111/geb.12701

Berdugo M, Delgado-Baquerizo M, Soliveres S et al (2020) Global ecosystem thresholds driven by aridity. Science 367:787. https://doi.org/10.1126/science.aay5958

Blumstein M, Gersony J, Martínez-Vilalta J, Sala A (2022) Global variation in nonstructural carbohydrate stores in response to climate. Global Change Biology n/a: https://doi.org/10.1111/gcb.16573

Bond WJ, Midgley JJ (2001) Ecology of sprouting in woody plants: the persistence niche. Trends Ecol Evol 16:45–51. https://doi.org/10.1016/S0169-5347(00)02033-4
Brodribb TJ, Powers J, Cochard H, Choat B (2020) Hanging by a thread? Forests and Drought Science 368:261. https://doi.org/10.1126/science.aat7631
Burlett R, Parise C, Capdeville G et al (2022) Measuring xylem hydraulic vulnerability for long-vessel species: an improved methodology with the flow centrifugation technique. Ann for Sci 79:5. https://doi.org/10.1186/s13595-022-01124-0
Burnham KP, Anderson DR (2003) Model selection and multimodel inference: a practical information-theoretic approach. Springer Science & Business Media
Choat B, Jansen S, Brodribb TJ et al (2012) Global convergence in the vulnerability of forests to drought. Nature 491:752–755
Choat B, Brodribb TJ, Brodersen CR et al (2018) Triggers of tree mortality under drought. Nature 558:531–539. https://doi.org/10.1038/s41586-018-0240-x
Cochard H (2002) A technique for measuring xylem hydraulic conductance under high negative pressures. Plant, Cell Environ 25:815–819. https://doi.org/10.1046/j.1365-3040.2002.00863.x
Dietze MC, Sala A, Carbone MS et al (2014) Nonstructural carbon in woody plants. Annu Rev Plant Biol 65:667–687. https://doi.org/10.1146/annurev-arplant-050213-040054
Duursma RA, Blackman CJ, Lopéz R et al (2019) On the minimum leaf conductance: its role in models of plant water use, and ecological and environmental controls. New Phytol 221:693–705. https://doi.org/10.1111/nph.15395
Felsenstein J (1985) Phylogenies and the comparative method. Am Nat 125:1–15. https://doi.org/10.1086/284325
Fox J (2002) Cox proportional-hazards regression for survival data. An R and S-PLUS companion to applied regression 2002
Freckleton RP, Harvey PH, Pagel M (2002) Phylogenetic analysis and comparative data: a test and review of evidence. Am Nat 160:712–726
Furze ME, Huggett BA, Aubrecht DM et al (2019) Whole-tree nonstructural carbohydrate storage and seasonal dynamics in five temperate species. New Phytol 221:1466–1477. https://doi.org/10.1111/nph.15462
Greenwood S, Ruiz-Benito P, Martínez-Vilalta J et al (2017) Tree mortality across biomes is promoted by drought intensity, lower wood density and higher specific leaf area. Ecol Lett 20:539–553. https://doi.org/10.1111/ele.12748
Hajek P, Link RM, Nock CA et al (2022) Mutually inclusive mechanisms of drought-induced tree mortality. Global Change Biology n/a: https://doi.org/10.1111/gcb.16146
Hammond WM, Yu K, Wilson LA et al (2019) Dead or dying? Quantifying the point of no return from hydraulic failure in drought-induced tree mortality. New Phytol 223:1834–1843. https://doi.org/10.1111/nph.15922
Hammond WM, Williams AP, Abatzoglou JT et al (2022) Global field observations of tree die-off reveal hotter-drought fingerprint for Earth's forests. Nat Commun 13:1761. https://doi.org/10.1038/s41467-022-29289-2
Hartmann H, Trumbore S (2016) Understanding the roles of nonstructural carbohydrates in forest trees – from what we can measure to what we want to know. New Phytol 211:386–403. https://doi.org/10.1111/nph.13955
Hartmann H, Bahn M, Carbone M, Richardson AD (2020) Plant carbon allocation in a changing world–challenges and progress: introduction to a Virtual Issue on carbon allocation. New Phytol 227:981–988
Hartmann H, Link RM, Schuldt B (2021) A whole-plant perspective of isohydry: stem-level support for leaf-level plant water regulation. Tree Physiol 41:901–905. https://doi.org/10.1093/treephys/tpab011
He W, Liu H, Qi Y et al (2020) Patterns in nonstructural carbohydrate contents at the tree organ level in response to drought duration. Glob Change Biol 26:3627–3638. https://doi.org/10.1111/gcb.15078
Hendriks JHM, Kolbe A, Gibon Y et al (2003) ADP-glucose pyrophosphorylase is activated by posttranslational redox-modification in response to light and to sugars in leaves of arabidopsis and other plant species. Plant Physiol 133:838. https://doi.org/10.1104/pp.103.024513
Herrera-Ramírez D, Sierra CA, Römermann C et al (2021) Starch and lipid storage strategies in tropical trees relate to growth and mortality. New Phytol 230:139–154. https://doi.org/10.1111/nph.17239
Huang J, Hammerbacher A, Gershenzon J et al (2021) Storage of carbon reserves in spruce trees is prioritized over growth in the face of carbon limitation. Proc Natl Acad Sci USA 118:e2023297118. https://doi.org/10.1073/pnas.2023297118
Jump AS, Ruiz-Benito P, Greenwood S et al (2017) Structural overshoot of tree growth with climate variability and the global spectrum of drought-induced forest dieback. Glob Change Biol 23:3742–3757. https://doi.org/10.1111/gcb.13636
Kassambara A, Kosinski M, Biecek P, Fabian S (2017) Package 'survminer.' Drawing survival curves using 'ggplot2' (R package version 03 1)
Li X, Piao S, Wang K et al (2020) Temporal trade-off between gymnosperm resistance and resilience increases forest sensitivity to extreme drought. Nature Ecology & Evolution 4:1075–1083. https://doi.org/10.1038/s41559-020-1217-3
Logan JA, Régnière J, Powell JA (2003) Assessing the impacts of global warming on forest pest dynamics. Front Ecol Environ 1:130–137. https://doi.org/10.1890/1540-9295(2003)001[0130:ATIOGW]2.0.CO;2
Magallón S, Gómez-Acevedo S, Sánchez-Reyes LL, Hernández-Hernández T (2015) A metacalibrated time-tree documents the early rise of flowering plant phylogenetic diversity. New Phytol 207:437–453. https://doi.org/10.1111/nph.13264
Mantova M, Menezes-Silva PE, Badel E et al (2021) The interplay of hydraulic failure and cell vitality explains tree capacity to recover from drought. Physiol Plant 172:247–257. https://doi.org/10.1111/ppl.13331
Mantova M, Herbette S, Cochard H, Torres-Ruiz JM (2022) Hydraulic failure and tree mortality: from correlation to causation. Trends Plant Sci 27:335–345. https://doi.org/10.1016/j.tplants.2021.10.003
Marshall JD (1986) Drought and shade interact to cause fine-root mortality in Douglas-fir seedlings. Plant Soil 91:51–60. https://doi.org/10.1007/BF02181818
Martínez-Vilalta J, Poyatos R, Aguadé D et al (2014) A new look at water transport regulation in plants. New Phytol 204:105–115. https://doi.org/10.1111/nph.12912
Martínez-Vilalta J, Sala A, Asensio D et al (2016) Dynamics of non-structural carbohydrates in terrestrial plants: a global synthesis. Ecol Monogr 86:495–516. https://doi.org/10.1002/ecm.1231
McDowell N, Pockman WT, Allen CD et al (2008) Mechanisms of plant survival and mortality during drought: why do some plants survive while others succumb to drought? New Phytol 178:719–739. https://doi.org/10.1111/j.1469-8137.2008.02436.x
McDowell NG, Sapes G, Pivovaroff A et al (2022) Mechanisms of woody-plant mortality under rising drought, CO_2 and vapour pressure deficit. Nature Reviews Earth & Environment 3:294–308. https://doi.org/10.1038/s43017-022-00272-1
Meinzer FC, Johnson DM, Lachenbruch B et al (2009) Xylem hydraulic safety margins in woody plants: coordination of stomatal control of xylem tension with hydraulic capacitance. Funct Ecol 23:922–930. https://doi.org/10.1111/j.1365-2435.2009.01577.x
Morcillo L, Muñoz-Rengifo JC, Torres-Ruiz JM et al (2022) Post-drought conditions and hydraulic dysfunction determine tree resilience and mortality across Mediterranean Aleppo pine (Pinus halepensis) populations after an extreme drought event. Tree Physiol 42:1364–1376. https://doi.org/10.1093/treephys/tpac001
Muller B, Pantin F, Génard M et al (2011) Water deficits uncouple growth from photosynthesis, increase C content, and modify the relationships between C and growth in sink organs. J Exp Bot 62:1715–1729. https://doi.org/10.1093/jxb/erq438
Myers JA, Kitajima K (2007) Carbohydrate storage enhances seedling shade and stress tolerance in a neotropical forest. J Ecol 95:383–395. https://doi.org/10.1111/j.1365-2745.2006.01207.x
O'Brien MJ, Leuzinger S, Philipson CD et al (2014) Drought survival of tropical tree seedlings enhanced by non-structural carbohydrate levels. Nat Clim Chang 4:710–714. https://doi.org/10.1038/nclimate2281
Orme D, Freckleton R, Thomas G et al (2018) Caper: comparative analyses of phylogenetics and evolution in R. R Package Version 1:1
Paradis E, Schliep K (2018) ape 5.0: an environment for modern phylogenetics and evolutionary analyses in R. Bioinformatics 1:3
Petek-Petrik A, Petrík P, Lamarque LJ et al (2023) Drought survival in conifer species is related to the time required to cross the stomatal safety margin. J Exp Bot 74:6847–6859. https://doi.org/10.1093/jxb/erad352
Powers JS, Vargas GG, Brodribb TJ et al (2020) A catastrophic tropical drought kills hydraulically vulnerable tree species. Glob Change Biol 26:3122–3133. https://doi.org/10.1111/gcb.15037

R Core Team (2020) R: a language and environment for statistical computing. R Foundation for Statistical Computing, Vienna
Rowland L, Da Costa ACL, Galbraith DR et al (2015) Death from drought in tropical forests is triggered by hydraulics not carbon starvation. Nature 528:119–122
Sala A, Piper F, Hoch G (2010) Physiological mechanisms of drought-induced tree mortality are far from being resolved. New Phytol 186:274–281. https://doi.org/10.1111/j.1469-8137.2009.03167.x
Sala A, Woodruff DR, Meinzer FC (2012) Carbon dynamics in trees: feast or famine? Tree Physiol 32:764–775. https://doi.org/10.1093/treephys/tpr143
Sanchez-Martinez P, Mencuccini M, García-Valdés R et al (2023) Increased hydraulic risk in assemblages of woody plant species predicts spatial patterns of drought-induced mortality. Nature Ecology & Evolution 7:1620–1632. https://doi.org/10.1038/s41559-023-02180-z
Sapes G, Roskilly B, Dobrowski S et al (2019) Plant water content integrates hydraulics and carbon depletion to predict drought-induced seedling mortality. Tree Physiol 39:1300–1312. https://doi.org/10.1093/treephys/tpz062
Sapes G, Demaree P, Lekberg Y, Sala A (2021) Plant carbohydrate depletion impairs water relations and spreads via ectomycorrhizal networks. New Phytol 229:3172–3183. https://doi.org/10.1111/nph.17134
Sevanto S, McDowell NG, Dickman LT et al (2014) How do trees die? A test of the hydraulic failure and carbon starvation hypotheses. Plant, Cell Environ 37:153–161. https://doi.org/10.1111/pce.12141
Smith SA, Brown JW (2018) Constructing a broadly inclusive seed plant phylogeny. Am J Bot 105:302–314. https://doi.org/10.1002/ajb2.1019
Smith AM, Stitt M (2007) Coordination of carbon supply and plant growth. Plant, Cell Environ 30:1126–1149. https://doi.org/10.1111/j.1365-3040.2007.01708.x
Stitt M, Lilley RMcC, Gerhardt R, Heldt HW (1989) [32] Metabolite levels in specific cells and subcellular compartments of plant leaves. In: Methods in Enzymology. Academic Press, pp 518–552
Thalmann M, Santelia D (2017) Starch as a determinant of plant fitness under abiotic stress. New Phytol 214:943–951. https://doi.org/10.1111/nph.14491
Tomasella M, Casolo V, Natale S et al (2021) Shade-induced reduction of stem nonstructural carbohydrates increases xylem vulnerability to embolism and impedes hydraulic recovery in Populus nigra. New Phytol 231:108–121. https://doi.org/10.1111/nph.17384
Torres-Ruiz JM, Cochard H, Delzon S et al (2024) Plant hydraulics at the heart of plant, crops and ecosystem functions in the face of climate change. New Phytol 241:984–999. https://doi.org/10.1111/nph.19463
Trueba S, Pan R, Scoffoni C et al (2019) Thresholds for leaf damage due to dehydration: declines of hydraulic function, stomatal conductance and cellular integrity precede those for photochemistry. New Phytol 223:134–149. https://doi.org/10.1111/nph.15779
Trueba S (2024) Nonstructural carbohydrates, water potential and mortality dynamics during drought in tree seedlings, [dataset], V1, Recherche Data Gouv. https://doi.org/10.57745/URI8QC
Urli M, Porté AJ, Cochard H et al (2013) Xylem embolism threshold for catastrophic hydraulic failure in angiosperm trees. Tree Physiol 33:672–683. https://doi.org/10.1093/treephys/tpt030
Weber R, Gessler A, Hoch G (2019) High carbon storage in carbon-limited trees. New Phytol 222:171–182. https://doi.org/10.1111/nph.15599
Zeeman SC, Kossmann J, Smith AM (2010) Starch: its metabolism, evolution, and biotechnological modification in plants. Annu Rev Plant Biol 61:209–234. https://doi.org/10.1146/annurev-arplant-042809-112301

Publisher's Note